

Aalto University
School of Engineering
Degree Programme in Marine Technology

Daniel Karlberg

The Effect of Three-dimensionality on the Radiation Forces of Surface Piercing Bodies

Master's Thesis
Espoo, February 17, 2014

Supervisor: Professor Jerzy Matusiak
Advisor: Tommi Mikkola, D.Sc.(Tech.)

Author:	Daniel Karlberg	
Title:	The Effect of Three-dimensionality on the Radiation Forces of Surface Piercing Bodies	
Date:	February 17, 2014	Pages: 81
Major:	Marine Technology	Code: Kul-24
Supervisor:	Professor Jerzy Matusiak	
Advisor:	Tommi Mikkola, D.Sc.(Tech.)	
	<p>In this thesis, the effect of three-dimensionality on radiation forces of surface piercing bodies is studied. This is carried out by using an existing Panel Method. The studied geometries are a rectangular barge, and a vertical flap, both in deep water.</p> <p>First, the potential flow, and the theory behind the used Panel Method are presented, together with an elaboration on the radiation terms, the added mass and damping.</p> <p>The effect of grid density on the results is studied, in order to minimize the errors related to the computational model. Sufficient grid resolutions are chosen for both of the geometries, and their different lengths.</p> <p>The studied modes of motion are sway, roll and heave. The results for added mass and damping, and their analysis is presented for the selected geometries and modes of motion.</p> <p>The main finding of this thesis is twofold: First, when a body is lengthened, the values of added mass and damping increase on average over the whole frequency range. Second, when the body is lengthened the characteristic behaviour of added mass and damping (embodied in the shape of the curve) moves towards lower frequencies. Due to this latter effect, although the values of added mass and damping increase on average when the body is lengthened, it can not be said that a lengthening of a body at a certain frequency automatically increases the values of added mass and damping.</p> <p>In the case of heave and roll for the studied geometries and frequencies, the convergence of added mass and damping to the 2D-solution takes place approximately when the body length L equals $20T$, T being the draught of the body. The three-dimensional behaviour of the added mass and damping of heave is more complex, and a clear convergence of the values as a function of length is not found.</p>	
Keywords:	potential flow, Panel Method, radiation-problem, three-dimensionality, added mass, damping	
Language:	English	

Tekijä:	Daniel Karlberg		
Työn nimi:	Kolmiulotteisuuden vaikutus radiaatiovoimiin vedenpinnan lävistävillä kappaleilla		
Päiväys:	17. helmikuuta 2014	Sivumäärä:	81
Pääaine:	Meritekniikka	Koodi:	Kul-24
Valvoja:	Professori Jerzy Matusiak		
Ohjaaja:	Tommi Mikkola, TkT		
<p>Tässä työssä tutkitaan kolmiulotteisuuden vaikutusta radiaatiovoimiin vedenpinnan lävistävillä kappaleilla. Tämä tehdään käyttäen olemassaolevaa paneelimenetelmää. Tutkitut kappaleet ovat suorakaiteen muotoinen proomu, sekä pystysuuntainen levy, molemmat asetettuna syvään veteen.</p> <p>Aluksi potentiaalvirtauksen sekä paneelimentelämän teoria esitellään, jonka jälkeen käsitellään lisätyn massan ja vaimennuksen olemusta.</p> <p>Mallinnetun verkon tiheyden vaikutusta tutkitaan, tavoitteena minimoida virheet, jotka liittyvät laskennalliseen malliin. Riittävät hilatiheydet valitaan kummallekin geometrialle, sekä niiden eri pituuksille.</p> <p>Tutkitut liikesuunnat ovat huojunta, keinunta sekä kohoilu. Lisätyn massan ja vaimennuksen tulokset sekä niiden analyysi esitetään valituille geometrioille, sekä niiden eri liikesuunnille</p> <p>Tämän työn päälöydökset voidaan ilmaista kahdella tavalla: Ensin, kappaleen pituutta kasvatettaessa lisätyn massan ja vaimennuksen arvot kasvavat keskimääräisesti mallinnettujen taajuuksien alueella. Toiseksi, kappaleen pituutta kasvatettaessa tutkitujen suureiden ominainen käyttäytyminen siirtyy kohti matalampia taajuuksia. Vaikka lisätyn massan ja vaimennuksen arvot kasvavat keskimäärin pituutta kasvatettaessa, jälkimmäisestä seurauksesta johtuen, ei voida sanoa, että kappaleen pidentäminen tietyllä taajudella automaattisesti kasvattaisi lisätyn massan ja vaimennuksen arvoa.</p> <p>Huojunnan ja keinunnan tapauksessa tutkitut suureet tutkituilla kappaleilla konvergoituvat kohti kaksiulotteista ratkaisua. Tämä tapahtuu likimain silloin, kun pituus L saavuttaa arvon $20T$, T:n ollessa kappaleen syväys. Kohoilun kolmiulotteinen käyttäytyminen on monimutkaisempaa, eikä selkeää konvergenssia voida sanoa olevan nähtävissä, tutkittujen kappaleiden eri pituuksilla.</p>			
Asiasanat:	potentiaalivirtaus, paneelimentelma, radiaatio-ongelma, kolmiulotteisuus, lisätty massa, vaimennus		
Kieli:	Englanti		

Acknowledgements

The research presented was carried out as a part of Fimecc's research program Innovations and Network and was funded by Tekes.

I want to thank my professor Jerzy Matusiak for his comprehensive and supportive approach as a professor, teacher and supervisor. I thank my instructor Tommi Mikkola for his insights, advice and precision regarding my whole thesis, as well as his time dedicated to this project.

Teemu Manderbacka and Otto Puolakka have been my friends on this journey towards graduation and completion of this thesis, and I thank them for that.

I am grateful to my family for their interest in me and my happiness. I thank my fiancée for her love and support during my entire studies.

Espoo, February 17, 2014

Daniel Karlberg

Abbreviations and Acronyms

α_{ji}	factor providing source contributions between panels j and i
β_{ji}	factor providing value of potentials at panel j due to contribution of panel i
Δ	displaced mass
δ	phase shift
η_0	wave amplitude
θ	horizontal angle
Λ_j	see equation (2.16)
λ	wavelength
μ	dynamic viscosity (of water)
ξ, η, ζ	coordinates of a source, notation corresponding to x, y, z
ρ	density (of water)
Φ	velocity potential in Green function representation
ϕ	velocity potential
ϕ_0	incident wave potential
ϕ_7	scattering potential
ϕ_j	velocity potential related to body motion to j th direction
ω_p	peak frequency for added mass or damping
ω	angular frequency of wave or motion
∇	vector differential operator, gradient
a	characteristic length of the structure, a non-dimensionalising factor
a_1	length of the first panel in geometric distribution
a_k	length of the k th panel in geometric distribution
B	body breadth
b_1	length of the first panel in even distribution
b_k	length of the k th panel in even distribution

d	depth of submergence, related to the origin of the body axis
F_j	force to j th direction, $j = 1, 2, 3$
F_{ji}	radiation force induced by i th motion to j th direction
F_j^0	force amplitude to j th direction
f	source strength on body surface
G	Green function
g	gravitational acceleration
h	water depth
h_j	normal components, see equation (2.15)
i	the imaginary unit or the index denoting direction
k	wave number
L	body length
M_{ji}	added mass induced by i th motion to j th direction
N_{ji}	damping induced by i th motion to j th direction
N	number of equations
\mathbf{n}	normal vector
p	pressure
p_{07}	diffraction pressure
p_j	radiation pressure on the surface of the body to each degree of freedom
p_{N11}	pressure contributing to added damping in sway
p_{M11}	pressure contributing to added mass in sway
q	geometric factor used in geometric panel distribution
r_1	horizontal distance
S	surface
ΔS	panel area
T	body draught (m)
T_w	wave period (s)
t	time
U	body velocity
u_j	velocity to j th direction, $j = 1, 2, 3$
\mathbf{v}	velocity vector of a fluid particle
\mathbf{v}_j	velocity vector of body motion in radiation problem
x_j	position in j th direction, $j = 1, 2, 3$
x_j^0	amplitude of body motion to j th direction
x	coordinate axis or value, interchangeable with x_1
y	coordinate axis or value, interchangeable with x_2
z	coordinate axis or value, interchangeable with x_3

Contents

Abbreviations and Acronyms	5
1 Introduction	9
1.1 The Linear Wave Theory	9
1.2 Solution methods	11
1.3 The scope of this work	12
2 The numerical method	14
2.1 The Potential Flow Theory	14
2.1.1 The motion of fluid	14
2.1.2 Free surface	16
2.2 The Green Function Method	17
2.2.1 The radiation problem	17
2.2.2 The diffraction problem	19
2.2.3 Solving the velocity potentials	20
2.3 The added mass and the damping	21
3 Studied cases	24
3.1 A circular cylinder	25
3.2 A rectangular barge and a vertical flap	26
3.2.1 The effect of grid-density	27
3.2.2 The process of elongation	28
3.2.3 The chosen factors	29
3.2.4 Verifying the results	30
4 Results	31
4.1 A circular cylinder - program verification	31
4.2 The effect of grid resolution	33
4.2.1 A vertical flap	33
4.2.2 A rectangular barge	37
4.2.3 Summary of the results regarding the grid resolution study	39
4.3 The effect of three-dimensionality	41
4.3.1 A swaying flap	42

4.3.2	A rolling flap	48
4.3.3	A swaying barge	53
4.3.4	A rolling barge	59
4.3.5	A heaving barge	64
4.3.6	The radiation pressures	68
5	Discussion	70
A	Flap radiation pressures	75

Chapter 1

Introduction

The interaction between water waves and a body in the sea is usually of interest to a naval architect, an ocean engineer, and to anyone working with marine hydrodynamics. However, this interaction is very complex and it is challenging to model it accurately. It is often necessary to make simplifications to the mathematical models that describe the flow or its characteristics. When simplifications are made -with proper justification- the problems become easier to solve. They do not require so much computational power or time. The downside of the simplifications, is usually the applicability of the method: It only works in certain situations with certain restrictions. For this reason, it is very important to know what the limitations of certain methods are, and when they can and cannot be used.

The aim of this work is to study the reliability of a method developed by Garrison (1974), for modelling forces acting on a surface piercing body in motion, to study the effect of three-dimensionality on these radiation forces and to shed light on the applicability of the method. Garrison's method is developed for large structures and it is based on the Linear Wave Theory. It uses a Boundary Element Method to solve the forces and motions in waves. The motivation for this account is to provide information for the research problems in Aalto University's department of Applied Mechanics. Additionally this account will shed light on the application possibilities of Garrison's method in general.

1.1 The Linear Wave Theory

In 1752, Leonhard Euler presented the *equation of continuity* as well as the concepts of *fluid pressure* and *velocity potential* (among other things). Soon after this, he derived the dynamic equations for ideal fluids, known today as the *Euler Equations*. Euler was influenced by Daniel Bernoulli, and was able to present in a sophisticated way some ideas Bernoulli had initially found.(Truesdell, 1953) The findings of Bernoulli and Euler are the very core of today's Potential Flow Theory.

In many marine applications it is usual to make the assumption that the fluid is ideal (incompressible, inviscid and irrotational) and therefore compliant to potential treatment. Incompressibility is a reasonable assumption, since seawater has a large elastic modulus (which describes the change of volume with respect to the change of pressure) of 2.34 GPa (Young et al., 2007). This means that the change of hydrostatic pressure from free surface to the depth of one kilometre, corresponds to the change of volume by -0.4 percent. Viscous effects (and rotation as a result) do play a role in many flows of marine applications, mainly through the formation of boundary layer and the flow separation. However, when sufficiently small amplitude motions are regarded, the assumption that the flow is inviscid is a good approximation (Garrison, 1974).

The presence of a free surface brings more complexity to the flow. In the case of surface waves that are treated with potential theory, it is customary to make the assumption that the wave amplitudes are small, which makes it possible to disregard the non-linear terms in boundary conditions of the velocity potential regarding the free surface (Newman, 1977). This linearisation leads to the so-called Linear (Airy) Wave Theory. The linearity allows superposition, which is very essential for the simplicity of the mathematical treatment of the problem. In Linear Wave Theory, the interaction of water and body is usually divided into two parts:

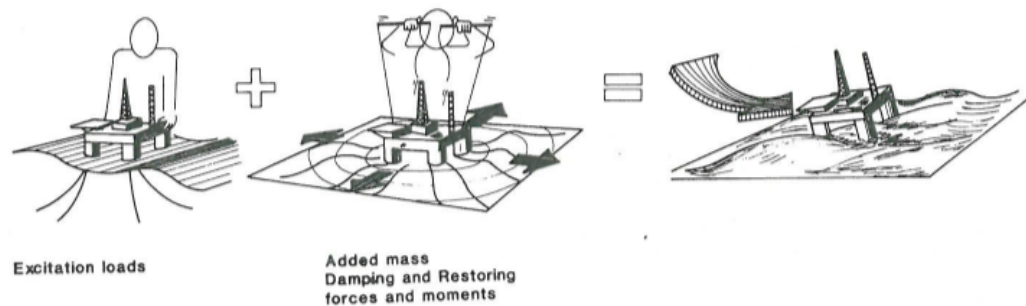


Figure 1.1: The wave-body interaction can be divided into two parts according to the Linear Wave Theory (Faltinsen, 1990).

1. The excitation problem, where the wave excitation forces are computed, while the body is held fixed in its position. This problem is commonly divided into two parts: the Froude-Krylov (the wave effect), and diffraction (the effect of diffracted waves).
2. The radiation problem, where fluid motion is caused by a body oscillating in otherwise still water, and the forces are expressed with the help of added mass and damping.

The summation of the radiation and excitation forces gives the total hydrodynamic forces acting on a body in the sea (Figure 1.1).

With Linear Wave Theory, it is possible to obtain results in the frequency domain. This means that the amplitudes of motions and forces can be presented e.g. as a function of the wave frequency. The result can be used in many ways, spanning from estimation of transmitted wave energy in frequency domain, to simulations of motions in time-domain.

1.2 Solution methods

The common way to solve the forces acting on a body in the sea, is the use of some kind of Boundary Element Method (BEM). This term is commonly used, also outside hydrodynamics, and can refer to an extended (weighted) version of the Finite Element Method, numerical implementation of boundary integral equation based on Green's formula, or a some sort of numerical method using boundary or boundary-like discretisation (Cheng and Cheng, 2005). In hydrodynamics, Boundary Element Methods that are used fall usually into two of the latter categories. Most commonly, the surface of the body is modelled by boundary elements (panels) and the flow field is solved around the whole body. Boundary Element Method and Panel Method are terms used interchangeably.

The first applications of Panel Methods occurred in the 1960s. In the 1970s they were still a novice method, but saw an exponential growth later on. The development and applications of BEMs, are also closely linked to the development of digital computers, which has enabled their use (Cheng and Cheng, 2005).

An example of the basic idea of a Panel Method is as follows: Elementary solutions of the Potential Theory (such as sources) are distributed e.g. on the body surface that is submerged and travelling at a constant speed. A boundary condition is given, which states: normal velocity through the body surface (panels), is the same as the body's velocity. The velocity potential of the whole problem is the sum of the free flow, as well as the velocity potentials of the panels (sources). The strength of the sources are unknown, but can be solved because of the known boundary conditions. When source strengths on all the panels have been obtained, the whole velocity field is known. Through the Bernoulli's Equation, the pressure distribution -and therefore forces (some being moments) to all degrees of freedom- can be solved.

There are mainly two kinds of boundary element (panel) formulations that are used in free surface problems: panels distributed only on the body surface (up to the free surface), or panels that are in addition to body surface distributed on the free surface as well. The former method uses Kelvin sources and the latter Rankine sources (Saisto, 1991). Strip methods are a

special case of the former method (that can also use analytical evaluation through conformal mapping), and are often used in the problems of ship seakeeping. In strip methods the body (ship hull) is divided into 10-30 slices (strips) and the boundary value problem is solved for each of the 2D-sections, and are summed up afterwards (Bertram, 2012). The limitation of strip methods is in their ability to model forces perpendicular to the cross sections. For shapes other than ships (where perpendicular forces are relevant), three-dimensional modelling is necessary.

Garrison's Panel Method is a Green Function Method where the sources are distributed only on the submerged body surface. The method is based on a general theory but the implementation in the computational routines is unique. The method is developed especially for large displacement structures, and it is able to model the hydrodynamic characteristics of both mounted, as well as free floating bodies. It is also capable of doing this in high frequency oscillation from 0.1 to 2.0 seconds (frequencies that mounted structures experience in earthquakes) and in ordinary gravity waves with periods that usually extend from 5.0 to 20.0 seconds (generally relevant for floating bodies).(Garrison, 1980)

1.3 The scope of this work

The radiation forces, represented using added mass and damping, are relevant quantities in ship dynamics and ocean engineering. This study focuses on these radiation forces, and examines their response to the lengthening of a body shape. Added mass is a quantity that describes the effect of accelerated water particles due to body motion. Damping is a quantity that describes the quantity by which energy is transferred from body motion to wave generation. Added mass and damping are the form, in which the solution to the radiation problem is usually presented (Figure 1.1). In the case of an arbitrary body, a Panel Method is an effective way to solve the radiation problem in three dimensions, presuming that the computational implementation in question works as it should.

For a hydrodynamicist, the effect of three-dimensionality on radiation forces can be very interesting, purely from a theoretical point of view. For anyone who is considering a length of a structure to certain sea conditions, this interest can take a practical form: What is the length that a structure should have, so that its response to the sea loads is optimum? The answer to the research question in this thesis can also be valuable information for anyone working with ships or ocean engineering in general. Wave energy applications are a new trade that might find use in these results as well.

In this study, two basic geometries, a vertical flap, and a rectangular barge, are modelled in different lengths using Garrison's Panel Method. The added mass and damping are computed for chosen wave-frequencies and the

results are studied in the light of the research question. First, however, it is confirmed that the program works as it should and that the grid resolutions used for modelling the different bodies suffice, so that the results can be held valid.

As stated before, the aim of this research is to confirm the validity of Garrison's Panel Method in computing the forces which act on surface piercing bodies in Airy Waves. The special interest of this study is the effect of three-dimensionality on the radiation forces of such bodies. In Chapter 2, the potential theory as well as the Garrison's Panel Method are presented. The studied cases and a grid resolution study related to them, are presented in Chapter 3. In Chapter 4, the results and an their analysis are presented. Discussion of the results is performed in Chapter 5.

Chapter 2

The numerical method

In this chapter, the Potential Flow Theory will be introduced. The effect of free surface in ideal fluid is discussed, and the equations behind the Panel Method are presented. Finally, the radiation forces - added mass and damping - will be discussed in more detail.

2.1 The Potential Flow Theory

The Potential Flow Theory is a theory regarding the flow of an ideal fluid. An ideal fluid is inviscid, irrotational and incompressible. The assumptions behind the Potential Flow Theory provide an effective way to represent and analyse flow, when viscous effects are negligible.

2.1.1 The motion of fluid

When the motion of fluid is modelled it is assumed that matter does not disappear. When fluid is travelling through an arbitrary control volume, a condition of mass continuity of the fluid can be obtained with elementary steps, yielding (Katz and Plotkin, 2001):

$$\frac{\partial \rho}{\partial t} + \nabla \cdot \rho \mathbf{v} = 0, \quad (2.1)$$

where ρ is density of fluid, t time, ∇ a vector differential operator and \mathbf{v} the velocity vector of a fluid particle. In this equation the compressibility is taken into consideration. However, in marine applications the compressibility does not have significance. It is a valid and fair assumption that the density ρ of water is constant. When this is assumed, (2.1) reduces to the form:

$$\nabla \cdot \mathbf{v} = 0, \quad (2.2)$$

or with alternative notation

$$\frac{\partial u_j}{\partial x_j} = 0, \quad i = 1, 2, 3, \quad (2.3)$$

where u denotes the velocity of a particle and x the position, both to j direction. The values of j refer to the axes x , y and z . In hydrodynamics this is known as the fundamental continuity equation.

The equations, which describe the flow without viscous effects are the previously derived continuity Equation (2.3) as well as an equation called the Euler equation (Newman, 1977):

$$\frac{\partial u_j}{\partial t} + u_j \frac{\partial u_i}{\partial x_j} = -\frac{1}{\rho} \frac{\partial p}{\partial x_i} + \frac{1}{\rho} F_i, \quad i = 1, 2, 3. \quad (2.4)$$

The left hand side of the equation represents acceleration and the right hand side represents forces divided by density ρ . The first term is the local acceleration of a particle. The second term describes the convective acceleration that takes place in relation to space. The third term describes the force induced by pressure and the fourth term describes the field force, which in marine applications is caused by gravity and equals ρg only to one direction of motion.

As was previously presented, the assumption that the water is incompressible and inviscid is reasonable for large bodies in the sea. The assumption that the flow is irrotational, can still be made. This assumption holds when

$$\nabla \times \mathbf{v} = 0, \quad (2.5)$$

everywhere in the fluid (Faltinsen, 1990). The term used for incompressible, inviscid and irrotational motion of fluid is *ideal flow*. For the ideal fluid, one is able to describe the flow with the help of a scalar function, whose gradient gives the velocity field. This function is also known as the velocity potential (usually denoted as ϕ), providing a basis for a whole approach to fluid motions that is known as the Potential Flow Theory. The velocity field is defined with the help of velocity potential as follows:

$$u_i = \frac{\partial \phi}{\partial x_i} \quad (2.6)$$

With the help of the velocity potential (2.6), the continuity equation (2.2) can be written to be

$$\nabla^2 \phi = \frac{\partial^2 \phi}{\partial x^2} + \frac{\partial^2 \phi}{\partial y^2} + \frac{\partial^2 \phi}{\partial z^2} = 0. \quad (2.7)$$

This form of an equation is fortunate, since it is a Laplace equation, a partial differential equation that can be solved when relevant boundary conditions are applied on the fluid (Faltinsen, 1990).

If there is a body in the fluid, from a kinematic point of view, it is important to note that the fluid will and shall not penetrate the body surface. For flow, which is described by the Potential Theory, this can be written as

Newman (1977) presents it:

$$\frac{\partial\phi}{\partial n} = \mathbf{U} \cdot \mathbf{n} \quad \text{on } S, \quad (2.8)$$

where S is the body surface and \mathbf{U} the body velocity.

2.1.2 Free surface

The presence of a free surface makes flow problems more complex. As is known, the real waves at sea are very irregular, propagating to many directions. Perfect modelling of such waves is impossible. In general, it can be stated that the longer the wave is in relation to its height, the easier it is to model it with reasonable accuracy. It has been found that the description of waves with potential theory can be quite accurate. There are two boundary conditions related to the free surface: kinematic and dynamic. It is common to linearise these conditions, and to obtain the so-called Linear Wave Theory. This linearisation allows superposition of solutions and the treatment of waves and wave effects both in time and frequency domain in a satisfactory manner. However, in order for this linearisation to take place and for it to be reasonable, small amplitude motions are assumed and required. The linearised kinematic boundary condition states that the normal velocity of a water particle needs to be of the same magnitude as the surface elevation. The linearised dynamic boundary condition states that the pressure on the water surface must be of the same magnitude as the air pressure. In addition, these are applied to the mean water surface (since small amplitude motions are in question, this can be done). When these conditions are joined, the combined free surface boundary condition for Linear Wave Theory is obtained (Garrison, 1978):

$$\frac{\partial\phi}{\partial y} - \frac{\omega^2}{g}\phi = 0 \quad \text{when } y = 0. \quad (2.9)$$

The solution for propagating waves needs to satisfy the continuity (2.7), as well as the free surface boundary condition (2.9). In addition to these, when the water is of finite depth, the following relationship needs to be met:

$$\frac{\partial\phi}{\partial y} = 0 \quad \text{at } y = -h, \quad (2.10)$$

where h is the water depth. There exists a solution for a potential function, which fulfills all of the conditions, equations (2.9), (2.7) and (2.10). Solutions can be derived for both finite and infinite depth. Newman (1977) presents the derivation of both of these, and the results can also be found in Faltinsen (1990).

2.2 The Green Function Method

Practical application of Potential Flow Theory comes through Boundary Element Methods, that are also known as Panel Methods. In these methods an arbitrary body is modelled through distribution of sources (in some cases dipoles or vortices) on the body surface. These sources are represented with panels that have a certain strength. The strength of these panels is highly relevant. What takes place in a Panel Method is that the source-strengths are solved in a way that fulfils all of the boundary conditions set to the fluid. When the source strengths are known, it is easy to obtain velocities and pressures wherever in the fluid and on the bounding surfaces. There are several Panel Methods, and different Green's function representations, depending on the application. For a free surface problem in the method in question, the Green function is presented for example in Garrison (1974).

Garrison (1974), (1978) presents a method utilizing the Green function and appropriate boundary conditions, in order to solve the motion of the fluid, forces and motion response of a large body in the sea. A traditional division enabled by linear theory is used, where the wave and body interaction is divided into two parts: the wave action on a stationary body (diffraction problem), and the motion of the body in still water (radiation problem). This division can be seen in Figure 1.1. The definitions used and the coordinate-system in Garrison's method are presented in Figure 2.1.

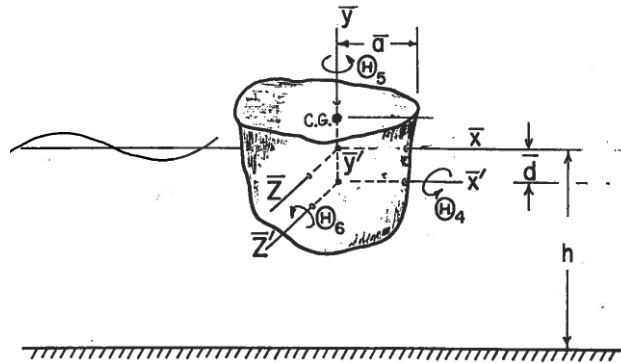


Figure 2.1: Definitions of the coordinate-systems in Garrison's method

2.2.1 The radiation problem

The motion of the body in the fluid (assumed small in comparison to its size) can be described with

$$x_j = x_j^0 \operatorname{Re}[e^{-i\omega t}], \quad j = 1, 2, \dots, 6 \quad (2.11)$$

where x_j^0 is the amplitude of the motion, t the time in seconds and ω the frequency of motion. Subscript j denotes the mode (degree of freedom) of

the motion. The velocities around the oscillating body can be described with the help of a potential function ϕ_j :

$$\mathbf{v}_j = \text{Re}[\nabla\phi_j e^{-i\omega t}], \quad j = 1, 2, \dots, 6, \quad (2.12)$$

where \mathbf{v}_j is the velocity vector. The pressures related to motions in every degree of freedom (j) can be described with the help of potential functions in the following manner (Garrison, 1974):

$$p_j = \rho\omega \text{Re}[i\phi_j e^{-i\omega t}], \quad j = 1, 2, \dots, 6. \quad (2.13)$$

In oscillation the no-penetration condition (2.8) in Garrison's (1978) method takes the following form at body surface S , where v_n is complex function representing body normal velocity:

$$v_n \equiv \frac{\partial\phi_j}{\partial n} = -i\omega x_j^0 h_j, \quad j = 1, 2, \dots, 6, \quad (2.14)$$

where h_j is defined as follows:

$$\begin{aligned} h_1 &= n_x, \\ h_2 &= n_y, \\ h_3 &= n_z, \\ h_4 &= (d+y)n_z - zn_y, \\ h_5 &= zn_x - xn_z, \\ h_6 &= xn_y - (d+y)n_x, \end{aligned} \quad (2.15)$$

when the unit normal vector on the surface $\mathbf{n} = \mathbf{i}n_x + \mathbf{j}n_y + \mathbf{k}n_z$ points outward from the surface into the fluid. Depth of submergence is denoted as d and is related to the origin of body axis origin (see Figure 2.1). These potentials are the solutions to the radiation problem. However, Garrison presents still one condition that needs to be fulfilled: The radiation condition which states that the only waves are the outgoing ones:

$$\phi_j(r, \theta, y) - \Lambda_j(\theta)r_1^{-1/2} \frac{\cosh[k(y+h)]}{\cosh(kh)} e^{ikr_1} \rightarrow 0, r_1 \rightarrow \infty, \quad (2.16)$$

where $r_1 = (x^2 + z^2)^{1/2}$ and $\theta = \tan^{-1}(z/x)$, wavenumber $k = 2\pi/\lambda$. The wave length, and the frequency of motion are related through dispersion relation

$$\frac{\omega^2}{g} = k \tanh(kh). \quad (2.17)$$

Equation (2.16) in infinite depth water takes form:

$$\phi_j(r, \theta, y) - \Lambda_j(\theta)r_1^{-1/2} e^{ikr_1} \rightarrow 0, r_1 \rightarrow \infty, \quad (2.18)$$

and the dispersion relation (2.17) simplifies to

$$\frac{\omega^2}{g} = k. \quad (2.19)$$

When the velocity potentials ϕ_j of the oscillatory motion are solved (see section 2.2.3) with the help of the Panel Method, the integration of pressures over the body surface S (eq. 2.13) give the force

$$F_{ji} = - \iint_S p_i h_j dS, \quad j, i = 1, 2, \dots, 6, \quad (2.20)$$

where the index j denotes the component of force that is induced by the i th component of body motion and h_j values are defined in equation (2.15). The common way of representing the forces in forced oscillation is with the help of added mass M_{ji} and damping N_{ji} .

$$F_{ji} = -M_{ji}\ddot{x} - N_{ji}\dot{x}. \quad (2.21)$$

The nature of the radiation terms - added mass and damping - that are central to the research question are discussed in Chapter 2.3.

2.2.2 The diffraction problem

When the interaction of a regular wave with a fixed body is regarded, the velocity potential can be written as

$$\phi_{07} = \phi_0 + \phi_7 \quad (2.22)$$

where ϕ_0 is the wave potential and ϕ_7 the potential of the scattered wave. With these potentials, the velocity vector of the fluid can be described as

$$\mathbf{v}_{07} = \text{Re}[\nabla(\phi_0 + \phi_7)e^{-i\omega t}] \quad (2.23)$$

and the pressures can be defined in the following manner:

$$p_{07} = \rho\omega \text{Re}[i(\phi_0 + \phi_7)e^{-i\omega t}] \quad (2.24)$$

The diffraction problem must satisfy the previously presented continuity (2.7) as well as the boundary conditions of the free surface (2.9), the bottom (2.10) and the radiation (2.16). In addition, the condition on the body surface -in comparison to equation (2.14)- takes form

$$\frac{\partial\phi_7}{\partial n} = -\frac{\partial\phi_0}{\partial n} \quad (2.25)$$

When ϕ_{07} is solved (see section 2.2.3) with the help of the Panel Method, the integration of pressure (eq. 2.24) over body surface S give the force

$$F_j = - \iint_S p_{07} h_j dS, \quad j = 1, 2, \dots, 6, \quad (2.26)$$

where the normals h_j can be found defined in equation (2.15).

2.2.3 Solving the velocity potentials

The solution for the diffraction and radiation problem can be obtained in similar manner. The only difference is the condition which is applied to the body surface. Depending on the problem, it is either (2.14) or (2.25).

The velocity potential with the distribution of sources can be expressed with velocity potential

$$\Phi = \frac{1}{4\pi} \iint_S f(\xi, \eta, \zeta) G(x, y, z; \xi, \eta, \zeta) dS \quad (2.27)$$

where x, y , and z denote the point in space (outside of the body surface) and ξ, η as well as ζ denote the point on the body surface S . For the source strength on the surface, notation $f(\xi, \eta, \zeta)$ is used. The Green function G represents a source potential that satisfies the linearised boundary condition at free surface, (2.9) as well as the conditions (2.7), (2.10), and (2.16) set to the fluid. The Green function G can be found for example in Garrison (1978).

For the radiation problem, when the kinematic boundary condition (2.14) is applied, following equations may be obtained.

$$-f_j + \frac{1}{2\pi} \iint_S f(\xi, \eta, \zeta) \frac{\partial G}{\partial n}(x, y, z; \xi, \eta, \zeta) dS = 2v_{n_j}, \quad (2.28)$$

where v_{n_j} is the body velocity corresponding to equation (2.14). When it is assumed that in each panel with area ΔS the source strength is constant over the panel, the surface integral can be evaluated as the sum of integrals over each panel:

$$-f_j + \alpha_{ji} f_i = 2v_{n_j}, \quad j, i = 1, 2, \dots, N, \quad (2.29)$$

where

$$\alpha_{ji} = \frac{1}{2\pi} \iint_{\Delta S_i} \frac{\partial G}{\partial n}(x_j, y_j, z_j; \xi, \eta, \zeta) dS \quad (2.30)$$

and the solution to this can be obtained with the help of matrix inverse

$$[f] = 2[\alpha - I]^{-1}[v_n]. \quad (2.31)$$

In a similar manner as above, equation (2.27) can be written as the sum of

$$\phi_j = \beta_{ji} f_i, \quad j, i = 1, 2, \dots, N, \quad (2.32)$$

where

$$\beta_{ji} = \frac{1}{4\pi} \iint_{\Delta S_i} G(x_j, y_j, z_j; \xi, \eta, \zeta) dS. \quad (2.33)$$

The diffraction problem is solved exactly in the same manner as the radiation problem through steps from equation (2.28) to (2.33). The only difference is that the condition applied to equation (2.28) is not (2.14), but (2.25) which means that the normal velocity component v_{n_j} is replaced by the wave potential derivative $\frac{-\partial\phi_0}{\partial n}$.

2.3 The added mass and the damping

Linear Wave Theory is a highly effective approach in computing wave motions, motions of body, and the forces on a body in relation to water with a free surface. For arbitrary bodies in three dimensions, a Panel Method is the way to carry out these computations. As presented before, the motions of a body are expressed as small amplitude oscillations (see Eq. 2.11). In fact, these motions are analogous to a harmonic oscillator. So much so that the body motions under the excitation of waves may be written in the following form (Matusiak, 2013):

$$(m_{ji} + M_{ji})\ddot{x} + N_{ji}\dot{x} + K_{ji}x = F_j^e, \quad (2.34)$$

where m_{ji} is the mass (or inertia) of the body, M_{ji} the added mass (or added inertia), N_{ji} the damping term and K_{ji} the restoring term (caused by buoyancy). F_j^e is the excitation force inducing the motions of the body to j th direction (see Eq. 2.26). The added mass and damping already presented in Equation (2.20), are the solutions to the radiation problem which is the central focus of this study. The effect of these forces on the motions under excitation may be seen in the light of equation the (2.34) presented above.

It is helpful to think of the motions in terms of a harmonic oscillator. In this way, the meaning of the terms is clarified. The added mass' effect is exactly the same as the inertial mass' effect on the motions. The effect of (added) damping is the same as the effect of a mechanical damper. However, usually in marine structures there is no mechanical damper and therefore, the only term affecting the motions through velocity is the damping related

to the body-water interaction. One aspect that should be noted is that the added mass and damping are not related to the body's mass or center of gravity. When the assumption of the small amplitude motions is held valid (a condition within Linear Wave Theory), the inter-dependence of the added properties is related only to the frequency of motion, the geometry of the body and the position of the body in relation to the free surface and the seabed.

A damper in a harmonic oscillator dissipates the energy (Inman, 2000) and the same takes place with the damping related to water. As a matter of fact, the kinetic energy of the body dissipated through the damping term equals the energy transmitted to wave-motion (Newman, 1977). In the case of an unbound fluid Newman (1977), explains that the added mass may be considered as a weighted average (based on acceleration) of the mass of the accelerated water particles, due to the motion of the body. In the light of these more or less physical explanations of the added mass and damping, perhaps the following may be stated: The damping term dictates how much energy is transferred from body motion to wave motion, and added mass describes what is the weighed average of the mass of the waterparticles that need to be accelerated so that this wavetrain can be set to motion in such a way, that all of the boundary conditions related to the fluid are met.

Newman (1977) also explains that for one mode of motion, there is a direct relation between the wave amplitude and the damping term. This relation can be derived when we know that the wave energy per wave length (in 2D) equals:

$$E_w = \frac{1}{2} \rho g A^2, \quad (2.35)$$

where A is the wave amplitude. The energy flux is obtained when the energy density is multiplied by the wave celerity c_g , which represents the speed at which the energy travels in the wavetrain:

$$P_w = \frac{1}{2} \rho g A^2 c_g \quad (2.36)$$

The work required to oscillate a body to one mode of motion and to generate radiating waves over one cycle is (Newman, 1977)

$$P_{rad} = \frac{1}{2} \omega^2 b_{jj} x_j^{02}, \quad (2.37)$$

where b_{jj} is the damping, and x_j^0 the amplitude of the motion to that direction. When it is set that $P_w = P_{rad}$ a relationship is obtained:

$$A = \frac{x_j^0}{g} \sqrt{\frac{\omega^3 b_{jj}}{\rho}}. \quad (2.38)$$

It can be seen that the amplitude of the generated wave depends on the amplitude of the motion, the damping coefficient and the frequency of the harmonic motion.

Chapter 3

Studied cases

In this Chapter, the studied geometries are presented. First, a circular cylinder (and its dimensions), which is used to verify the programs ability to perform as it was designed. Then, the two geometries (a rectangular barge and a vertical flap), and their lengths that are studied. This chapter also presents the way that the grid is defined for both of the latter geometries, and how the reliability of the results for the added mass and damping with these grid-resolutions can be confirmed.

It is important to note the used coordinates (Figure 3.1) in this study. The coordinate-system is right-handed and the y-axis points upwards. The length of the body extends in z-direction, and the breadth to x-direction. In the computations of this study, sway takes place along x-axis, heave along y-axis, and the roll around the z-axis. The numbers referring to these modes of motions are 1,2 and 6, respectively. The reason for these choices has been affected by two things: the coordinate system of Garrison's program, as well as the simplicity of modelling.

The studied cases are all symmetrical with respect to both xy- and zy-planes. This means that only one fourth of the geometry in question requires modeling as an input into the Garrison's program. The program mirrors the modelled quarter to correspond to the whole geometry. Each panel (also in the mirrored part) affects the other panels. The results for the added mass

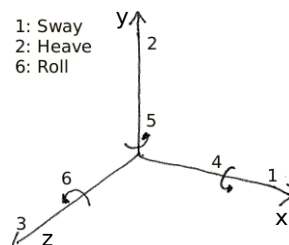


Figure 3.1: The used coordinates and terms for different modes of motions.

and damping are obtained in one quarter (the modelled one), after which they can be extrapolated by mirroring them to the rest of the quarters.

3.1 A circular cylinder

Garrison (1975, p. 62) presents results for a circular cylinder computed using his method. A lot has happened since the paper was published. It is a good idea to confirm that the program he has written still performs in a similar manner in the computers and compilers of today. Garrison's program has also been at the Aalto University (former Helsinki University of Technology) and has gone through some development, which might have an effect on how the program works. It is not known with how many panels Garrison has modelled his cylinder, nor what dimensions he has used. Regardless of this, it is expected that when a circular cylinder is modelled with some sufficient panel arrangement, the results should be close to those of the ones in the paper by Garrison (1975). The dimensions of the cylinder can be found in Figure 3.2. The circular cylinder has a radius a and is placed in water with the draught of $\frac{a}{2}$.

Let three different panel resolutions be used to model the cylinder (Figure 4.1) and compare the results of added mass and damping with the results obtained by Garrison. The grid refinement is done, so that the possible errors from used grid resolutions could be revealed. The studied quantities for the circular cylinder are the added mass and damping of sway and heave. The results can be found in section 4.1.

The results for the cylinder are made non-dimensional. The added mass is divided by ρa^3 , where ρ is the water density, and a the radius of the cylinder. The damping is divided by $\rho a^3 \omega$, where ω is the oscillation frequency.

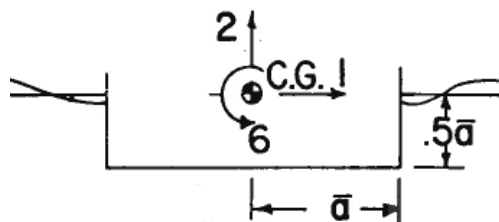


Figure 3.2: Circular cylinder sideview, numbers denoting the degrees of freedom used in Garrison's method (Garrison, 1975).

3.2 A rectangular barge and a vertical flap

There are two cases in which the effect of the length of a body on radiation forces will be studied. The first is a vertical plate, with B/T ratio of $1/8$. The second geometry is a rectangular barge, where the same ratio is $2/1$. Front view of these geometries can be seen in Figure 3.3. These geometries are inherently different. Therefore, the results for added mass and damping for both geometries can increase the understanding of the more general effect that the lengthening (or three-dimensionality) has on these radiation forces.



Figure 3.3: The two different cross-sections to be studied. A vertical plate (red) with B/T ratio of $1/8$, and a rectangular barge (blue) with B/T ratio of 2 .

The lengths are chosen in relation to the draught of the body. These chosen lengths are $T/2$, T , $2T$, $3T$, $5T$, $10T$, $20T$ and $50T$ (Figure 3.4). In general, the approach is such that a period spectrum from 3 to 20 seconds is chosen. These periods easily cover the most common wave frequencies occurring in the seas. The bodies are modelled in such a way, that the chosen draught is 8 meters, and the breadth varies accordingly. The B/T of $1/8$ is somewhat randomly chosen, but with this type of a geometry, the force induced by horizontal movement (sway) is relatively large and interesting to study. There are such geometries e.g. in shallow water, which are being developed for wave energy conversion. Although the computations in this thesis are conducted in deep water, the results most probably give an indication of the force behaviour in shallow water as well. The B/T ratio of 2 is a realistic one for ship types such as tankers. For this ratio there is also reference data in 2D (Vugts, 1968), and it is possible to compare the present results with those.

The added mass and damping of the vertical flap are studied in sway and roll. The added mass and damping of the rectangular barge are studied in sway, roll and heave. The results for both of the geometries are made non-dimensional similarly.

The added mass of sway and heave is divided by the body's displacement mass Δ . The damping of sway and heave is multiplied by $\sqrt{\frac{T}{g}}/\Delta$, where T is the draught of the body, and g the gravitational acceleration.

The added mass of roll for both of the geometries, is made non-dimensional by dividing it by ΔB^2 , where B is the breadth of the body. The damping of roll for both of the geometries, is made non-dimensional by multiplying it by $\sqrt{\frac{T}{g}}/(\Delta B^2)$.



Figure 3.4: The studied lengths for both cross-sections

3.2.1 The effect of grid-density

Because of the nature of the problem in this thesis (the effect of the length on radiation forces), it is important to eliminate the errors that are related to the panel arrangement and its variation. It is not possible to use even distribution of panels to the longitudinal direction (parallel to z-axis) because for the longer bodies either the amount of panels would become uncomputable (short panels) or the results inaccurate (long panels). One option is to use a geometric series. However, the mere use of a such series in the longitudinal panel distribution does not come into question either, since the ratio between the shortest and longest length of a geometry is 100 (see Figure 3.4). This means that obtaining high accuracy with the longest bodies close to the edge, would mean either very long panels at the center of the geometry or a very large amount of panels for the whole geometry. Due to these factors, it is seen that the best approach is to use a hybrid solution, where up until a certain length, the geometries are modelled with a geometric series in the longitudinal direction after which an even distribution is applied for the portion that exceeds this chosen length (Figure 3.5). At this point it should again be noted that of all the following body geometries, only one fourth is modelled. In which case the complete geometry is the modelled part, mirrored through both the y-z and the x-y planes. A general choice is made, where the panel length cannot exceed one tenth of a computed wave-length (Eq. 3.1). This is to assure that pressures and velocities over a wavelength can be described in the program in a realistic manner:

$$L_{panel} < \frac{\lambda}{10}. \quad (3.1)$$

In the panel implementation, the geometric series takes the form of

$$a_k = a_1 \cdot q^k, \quad q > 1, \quad k > 1 \quad (3.2)$$

where a_1 is the length of the first panel and a_k the length of the k th panel. The geometric factor is denoted as q . The even distribution is a special case

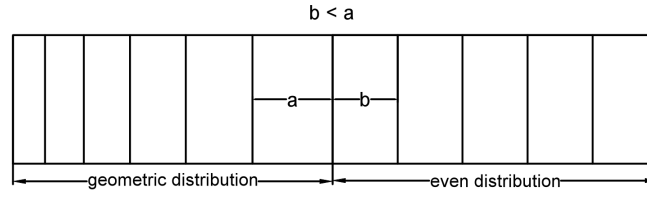


Figure 3.5: An example of a hybrid solution for the longitudinal panel distribution. To ensure accuracy, the panels in even distribution are made shorter than the last panel of the geometric distribution.

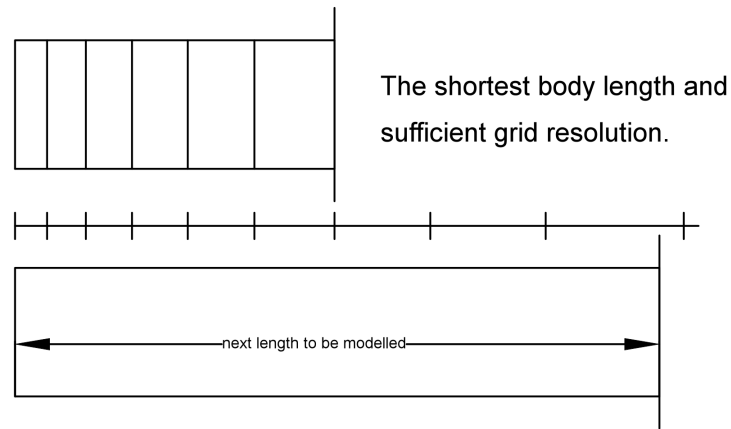
of the geometric distribution, where the geometric factor $q = 1$ and therefore (3.2) takes form.

$$b_k = b_1, \quad k > 1. \quad (3.3)$$

Purposefully, the letters denoting the length of a panel were changed in order to avoid confusion between the geometrically distributed and evenly distributed panels. The length of each panel b_k equals b_1 in the evenly distributed part of the body.

3.2.2 The process of elongation

When the body is elongated, the aim is to hold the end of the geometry as unchanged as possible, in terms of panel distribution. This means that when two body lengths are compared to each other, the longer body has the shorter body's panels up until the length of the shorter body. When a geometric distribution is in question, this requirement cannot be fully met. This means that some small compromises need to be made. The elongation process goes as follows: First, a proper panel distribution is found for the shortest lengths ($1/2T$) by estimating a sufficient grid density (including a geometric factor) and then systematically refining the grid. When the results can be seen to converge, a proper grid resolution (including the geometric factor) can be chosen to model the body at the shortest length ($1/2T$). Secondly, the length of the body is increased to match the chosen lengths (see Figure 3.4). When the length is increased, the longitudinal panel amount is chosen by a geometric series (where the geometric factor is now held unchanged) in such way, that the panel amount which first exceeds the desired length for the structure, is chosen to model the body (see. Figure 3.6). When the elongation takes place in this way, the lengths of the panels (also close to the body edge) vary slightly, but never is their length greater than what was initially chosen for the sufficient accuracy for the shortest length. Third, to make sure that this kind of elongation process does not affect the accuracy of the results, a grid refinement is performed again, but for the geometry that is the last to be modelled purely with the geometric distribution. Provided that the results for this length are well converged, the method of lengthening



The geometric factor is held unchanged, but the panel lengths are scaled down

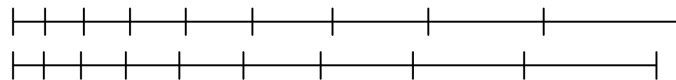


Figure 3.6: Schematic representation of the elongation process with body lengths modelled with geometric distribution.

as well as the results for the bodies between these two lengths, may be considered valid.

3.2.3 The chosen factors

For both of the body cross-sections (barge and flap), the first panel arrangement is chosen with common sense, assuming that it could give accurate enough results. The geometric factor in the longitudinal direction is chosen to be 1.2 and found to give reasonable results for both body-shapes. The longest length that can be modelled with this geometric factor without violating the panel length condition (3.1) is $5T$. This means then that for the bodies with lengths $10T$, $20T$ and $50T$, the part that exceeds $5T$, is modelled with an even distribution.

For lengths that are modelled both with the geometric and the even distribution, the aim is to set the length of an evenly distributed panel to be the same as the last panel length of the $5T$ long geometry. However, this is not possible with the chosen lengths, and therefore a condition is set, where these panels are shorter than the longest panel of the $5T$ long geometry (see also Figure 3.5):

$$a_k > b_1. \quad (3.4)$$

This is to ensure the accuracy of the results.

3.2.4 Verifying the results

The amount of panels in the grid resolution study for the length $1/2T$ (both a rectangular barge as well as a vertical flap) is increased twice by the factor of $\sqrt{2}$ to each direction. It is assumed that this refining will show the convergence of results. The same is carried out for the length $5T$. At this length in the longitudinal direction, however, instead of maintaining the geometric factor 1.2, the factor is adjusted so that the ratio between the first and the last panel remains constant. This is seen to be necessary, so that all the panels shrink a desirable amount. The results of this study can be found for both geometries in section 4.2.

Chapter 4

Results

4.1 A circular cylinder - program verification

The results for the circular cylinder are presented here. The different grid resolutions can be seen in Figure 4.1 and the added mass and damping for those in Figures 4.2 and 4.3.

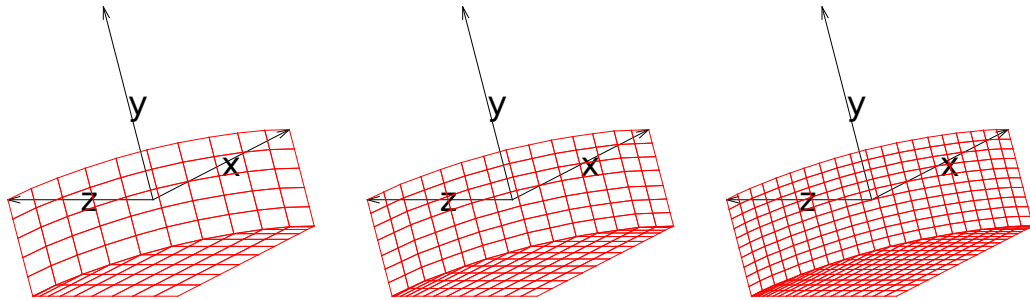


Figure 4.1: Cylinder panel resolutions in quarter of the body: 105; 203 and 410. Water surface at xz-plane.

in general, the results appear to match the ones of Garrison (Figures 4.2 and 4.3), although some deviations can be seen.

In sway, the added mass follows the Garrison's curve faithfully. However, there are some deviations at the both ends of the computational domain. It is unclear what causes these. Due to the fact that the results seem to converge at these ends smoothly, it is unlikely that the reason is in the panel-sizes. The damping of sway has the very same form as Garrison's computation. The only difference is in the peak value and the surrounding domain close to this. However, the error is relatively small.

In heave, the curves for added mass and damping correspond exactly to the results that Garrison has obtained, apart from the very lowest frequencies in the added mass. Garrison did not compute these added mass

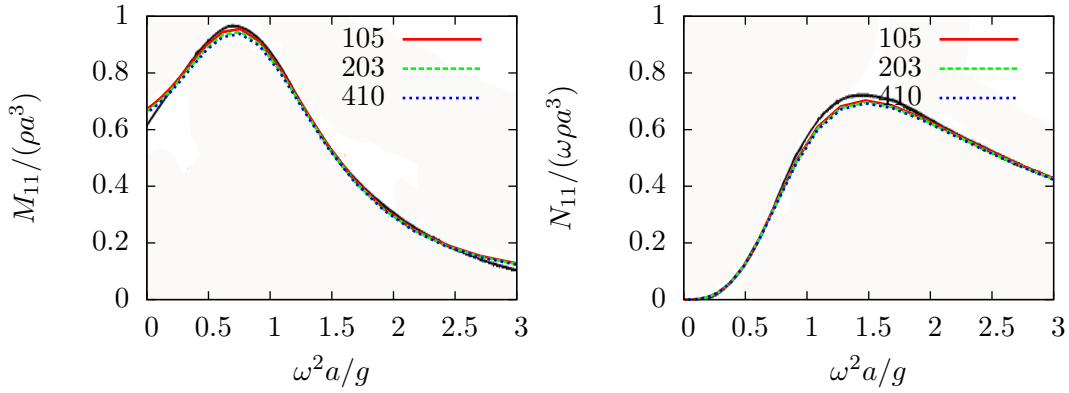


Figure 4.2: Circular cylinder in sway, added mass and damping. A comparison of computation results with Garrison's (1975) original ones (black line) with panel resolutions 105, 203 and 410.

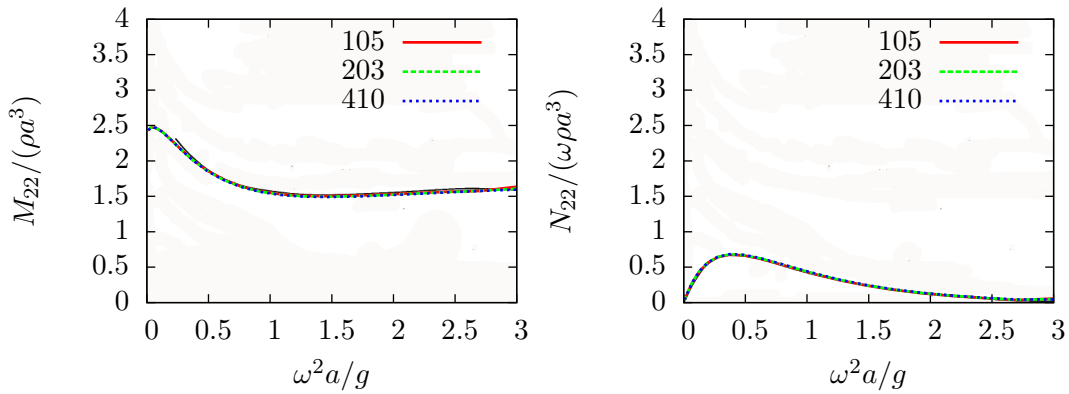


Figure 4.3: Circular cylinder in heave, added mass and damping. A comparison of computation results with Garrison's (1975) original ones (black line) with panel resolutions 105, 203 and 410.

values starting at zero, and the starting point around 0.25 of the dimensionless frequency gives a value deviating from the present computations. This deviation, as were the previous ones, is a small one.

Despite the small differences in some of the quantities, the agreement of results is good and the program seems to perform as it was designed to. In this light, the study of the effect of three-dimensionality on radiation forces can be continued with the help of the Garrison's program.

4.2 The effect of grid resolution

In this section the results for the effect of the grid refinement on added mass and damping in different modes of motion are presented for both body cross-sections, the flap and the barge.

4.2.1 A vertical flap

The grid resolution study for the vertical plate is performed in two modes of motion, sway and roll. The forces in the direction of heave have been omitted, as they are so small and rarely of interest. The studied grid resolutions for the length $1/2T$ are 80, 184 and 370 panels (Figure 4.4) and for the length of $5T$ they are 257 and 524 and 1066 panels (Figure 4.5). The results for added mass and damping for the aforementioned modes of motion and body lengths can be found in Figures 4.6 and 4.7.

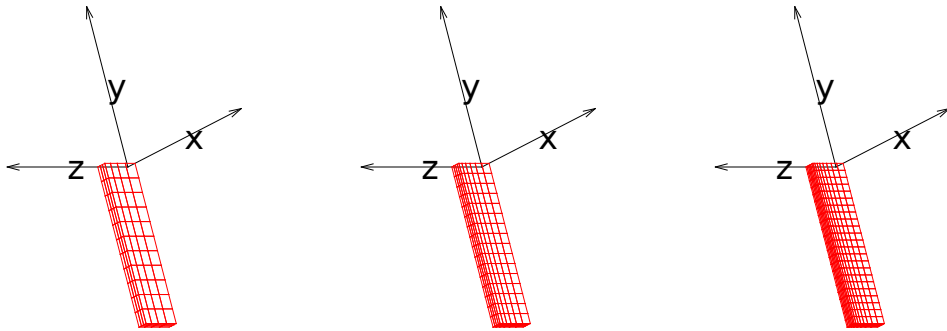


Figure 4.4: Flap with the length of $1/2T$ with grid resolutions corresponding 80, 184 and 370 panels in the quarter a body. Water surface at xz -plane, body length to z -direction.

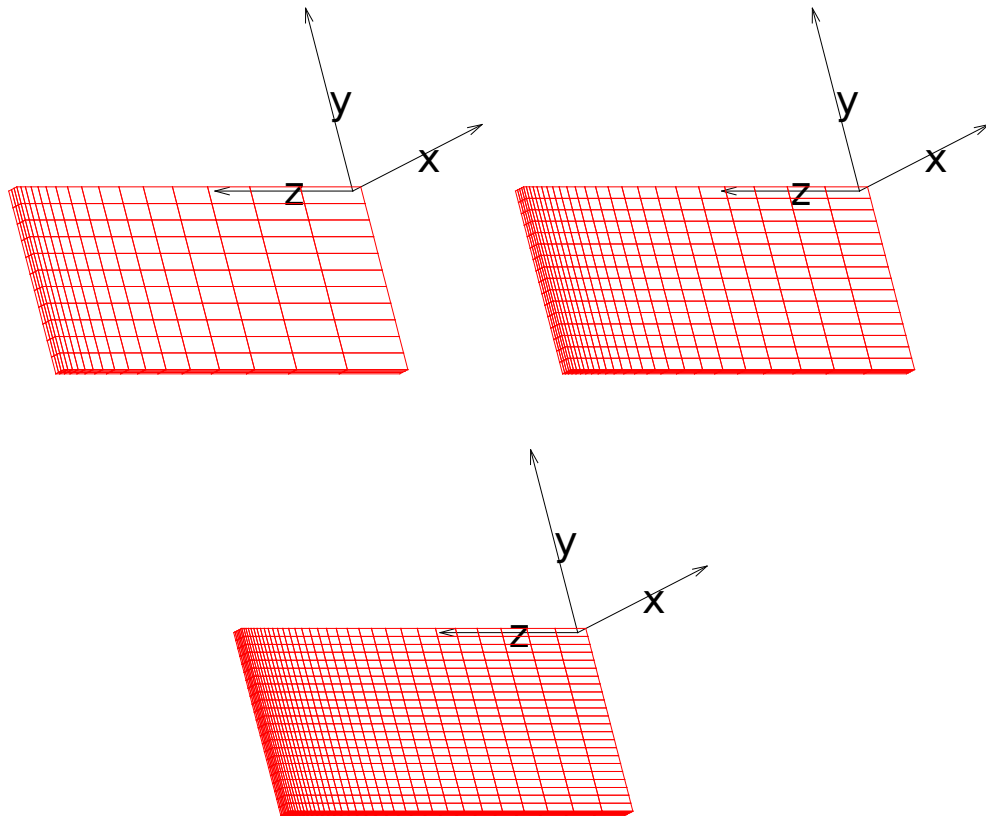


Figure 4.5: Flap with the length of $5T$ with grid resolutions corresponding 257, 524 and 1066 panels in the quarter a body. Water surface at xz -plane.

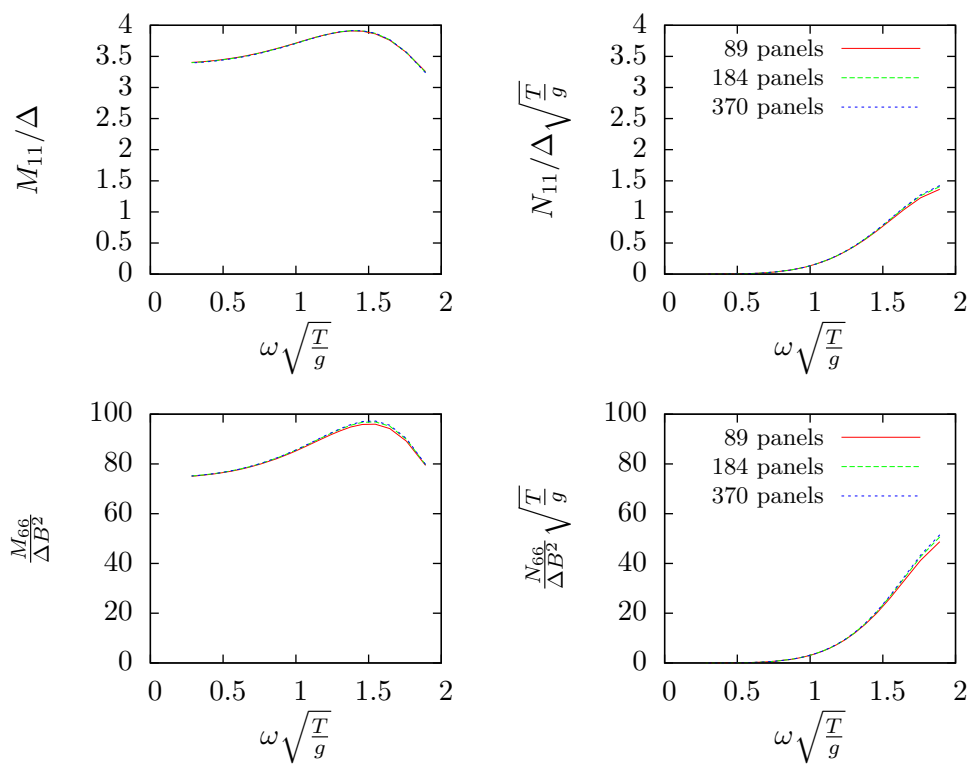


Figure 4.6: $1/2T$ long flap in sway and roll with different panel resolutions. Added mass and damping.

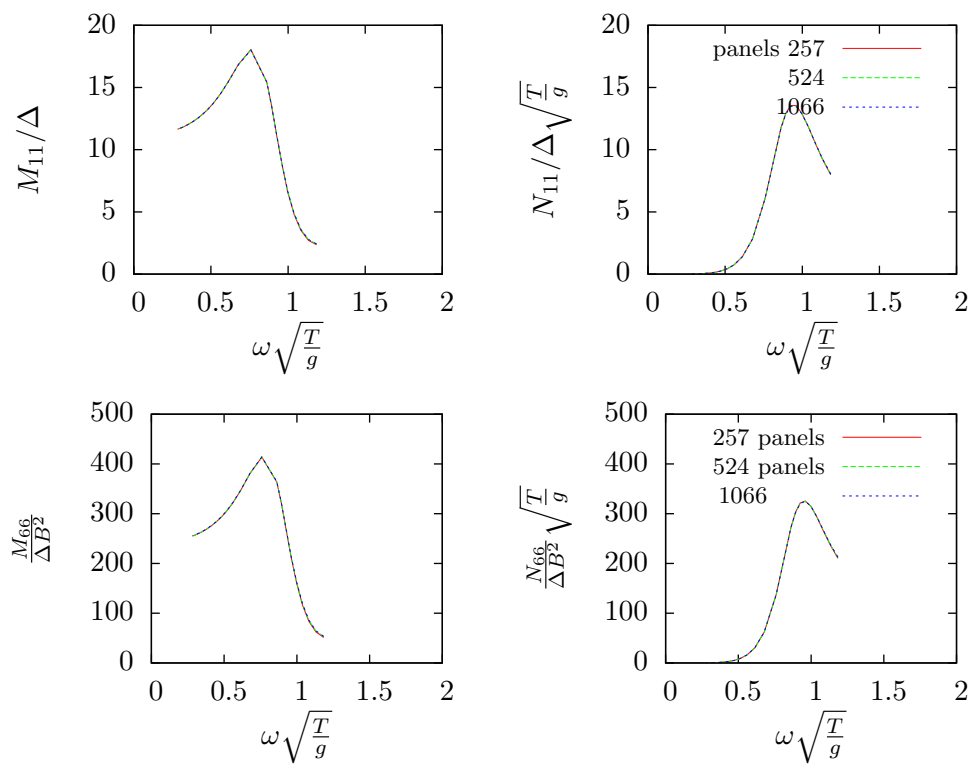


Figure 4.7: $5T$ long flap in sway and roll with different panel resolutions. Added mass and damping.

4.2.2 A rectangular barge

The grid resolution study for a rectangular barge is performed in three modes of motion, sway, heave and surge. The studied grid resolutions for the length $0.5T$ are 209, 448 and 897 panels (Figure 4.8) and for the length of $5T$ they are 473 and 992 panels (Figure 4.9). The reason for only two studied cases for the $5T$ long body is the rapidly increasing computational time. It is seen that a third resolution is not necessary for the verification of the results. These results for added mass and damping for the aforementioned modes of motion and body lengths can be found in Figures 4.10 and 4.11.

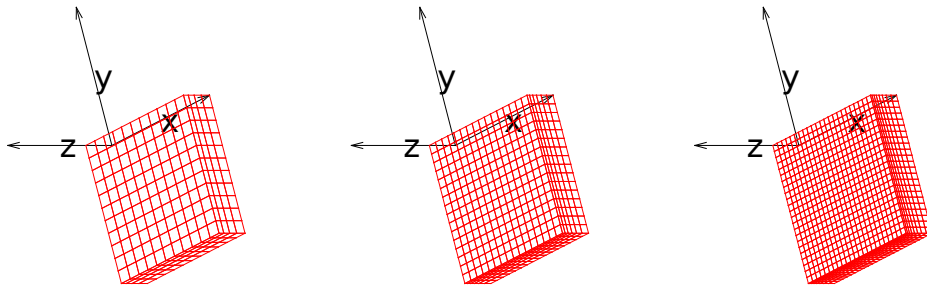


Figure 4.8: Different grid arrangements to model a rectangular barge with length of $T/2$. Grid resolutions in quarter of a body, from left to right: 209, 448 and 897 panels. Water surface at xz -plane, body length to z -direction.

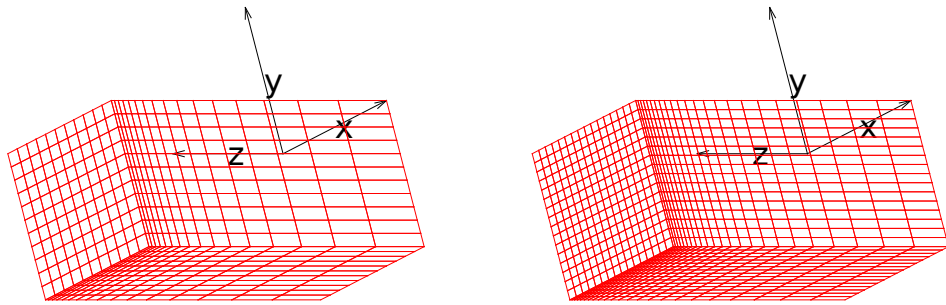


Figure 4.9: Case 43 with 473 panels and Case 44 with 992 panels. Water surface at xz -plane.

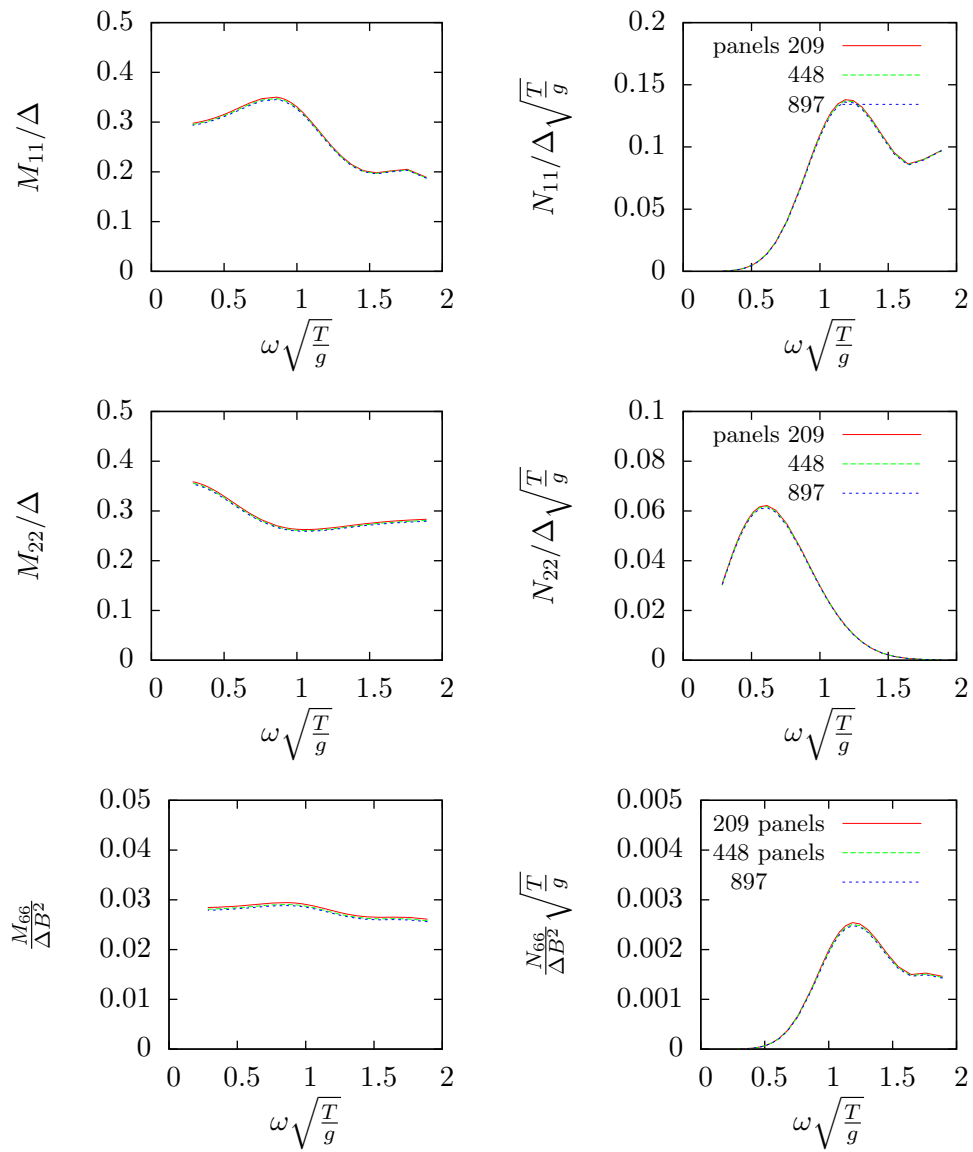


Figure 4.10: $1/2T$ long rectangular barge in sway heave and roll with different panel resolutions. Added mass and damping.

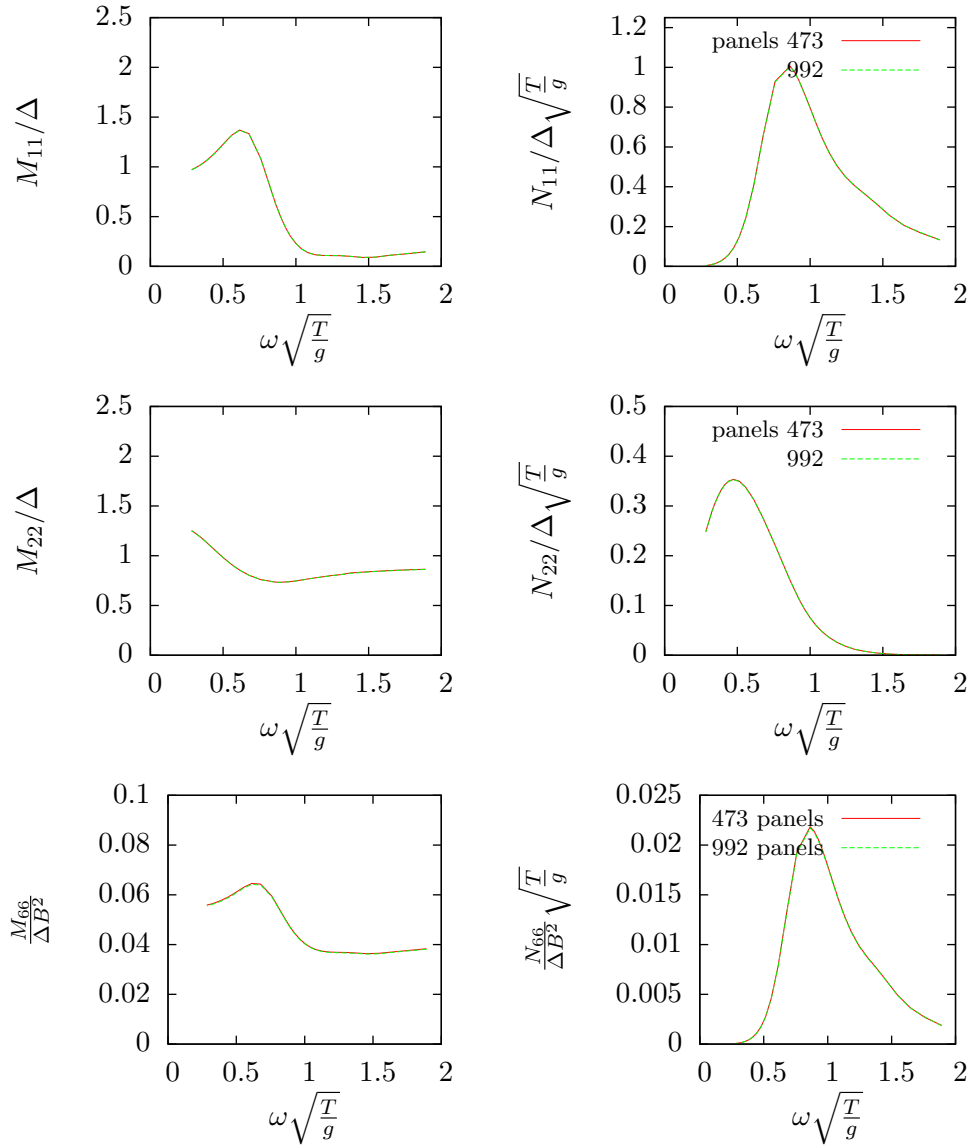


Figure 4.11: $5T$ long rectangular barge in sway, heave and roll with different panel resolutions. Added mass and damping.

4.2.3 Summary of the results regarding the grid resolution study

The results for added mass and damping are very close to each other, for both the rectangular barge as well as the vertical flap. This suggests that the lowest grid resolutions used in this study can be used to model the geometries. It is clear that since the results are converged with these arrangements

for the lengths $1/2T$ and $5T$, there is no significant grid dependence for the lengths inbetween these studied cases either. Despite the fact that the curves seem to be on top of each other, a converging behaviour can still be found. The difference in the values of added mass and damping are smaller between the two highest grid resolutions, in comparison to the two lowest resolutions. These results also indicate that the results in general are very close to the results that can be obtained with a infinitely dense grid. Based on these findings, it can be said that the effect of length on the radiation forces can be studied with the lowest of the used resolutions, and that the reliability of those results is established.

4.3 The effect of three-dimensionality

The results here are presented first for the flap-geometry, then for the barge-geometry. The studied quantities are the sway and roll added mass and damping, as well as the heave added mass and damping for the rectangular barge. The presented results attempt to answer the research-question: the effect of three-dimensionality on radiation forces. The results are presented in the form of graphs, one geometry and one mode of motion at a time. An analysis follows, after each geometry and each mode of motion. A more general discussion, elaboration on the common characteristics of the results, and the conclusions are drawn in Chapter 5. The results also include a part where the added mass and damping distribution (radiation pressures), is studied with the help of sway of the flap geometry. The graphs themselves are presented in the Appendix (A), but an analysis of them is presented as a part of this Chapter (4.3.6).

The general approach for presenting the results for both geometries, and their modes of motion in this section is as follows:

1. The added mass and damping as a function of frequency: comparison of the results between the different lengths and possible 2D-solutions.
2. A presentation of the peak values of added mass and damping and their frequencies as a function of body-length.
3. The added mass and damping as a function of length: a comparison of the curves between the three chosen frequencies.

It should be noted that the added mass and damping for flap's roll motion is computed around the point situated at depth $y = -T$, but for the rectangular barge at water level ($y = 0$).

4.3.1 A swaying flap

The results for a swaying flap are presented in this section. An analysis of these results is presented together with the graphs. Sway is the motion to x-direction, perpendicular to the length of the structure. The B/T ratio of a flap is $1/8$. Schematic presentation of the situation is seen in Figure 4.12.

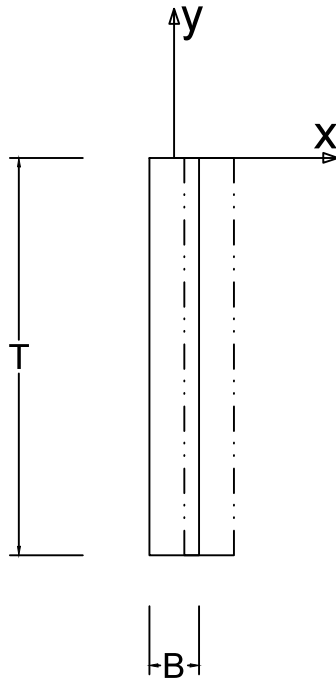


Figure 4.12: A schematic presentation of the swaying flap.

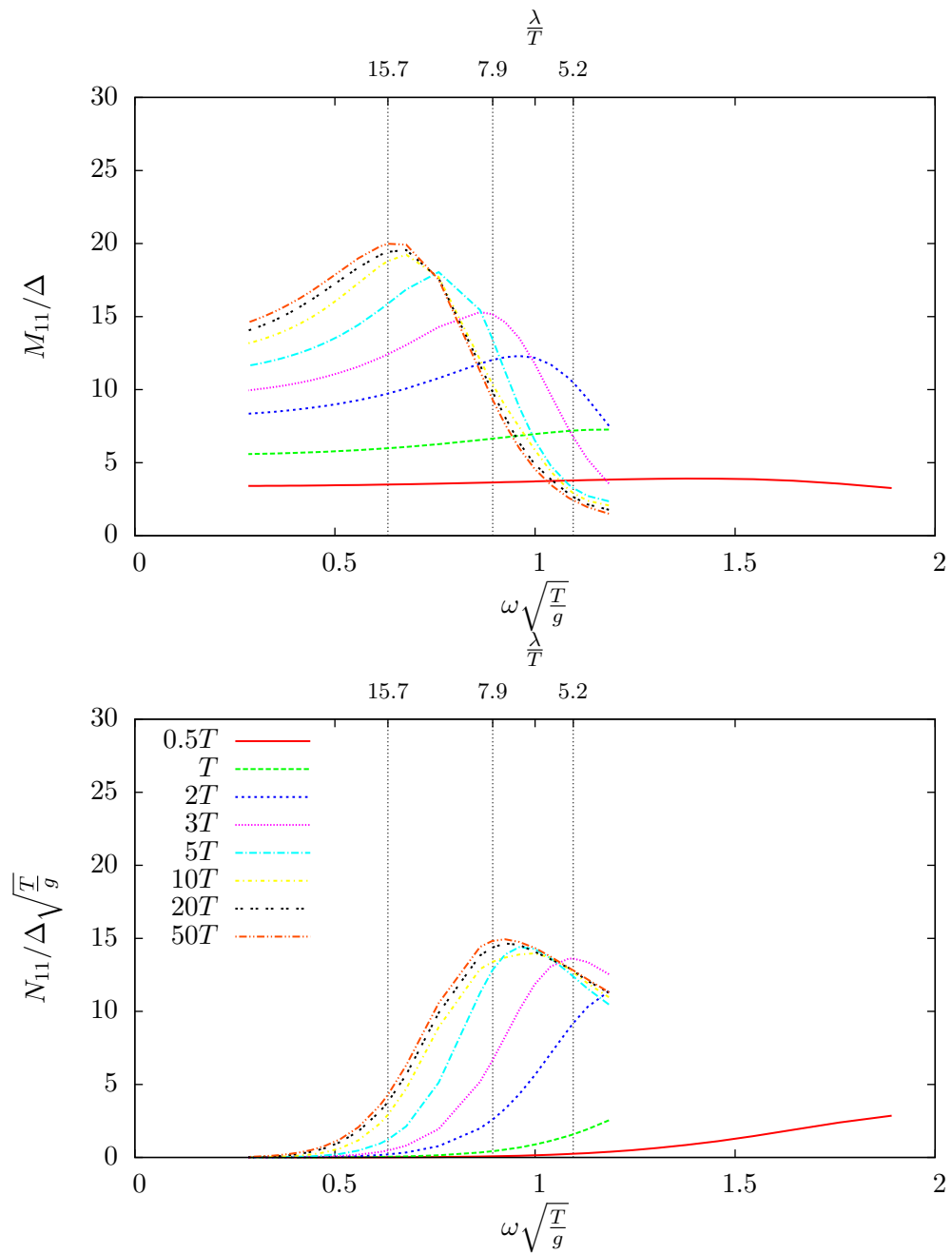


Figure 4.13: Flap sway added mass (above) and damping as a function of the dimensionless frequency with different body lengths.

For the longest length ($50T$) (Figure 4.13) that can be assumed to be close to the 2D-solution, the added mass increases up until the peak value when the frequency of motion is increased. At the same time the damping increases and when its derivative is at its highest, the added mass starts to decrease. This takes place linearly, and then in a decelerating manner, but approaching zero. The change from constant to decelerating decrease takes place around the frequency of the damping's peak value. It is interesting to observe that the behaviour of added mass and damping in relation to frequency have the same nature, regardless of the length of the body (Figure 4.13). This is to say that the behaviour as such does not differ much from the longest length, when the length is decreased. However, what can be noticed is that the added mass per unit length decreases clearly when the length is decreased.

There is a "phase shift" that can be noticed, in both of the quantities. This is to say that the characteristic behaviour shifts more to right, towards higher frequencies, when the length decreases. The general consequences of these shifts are that the added mass per displacement for a smaller body length, can be larger than that of a larger body length with a frequency that is higher than the larger body's added mass peak value frequency. Although the damping term per displacement does not decrease proportionally as much as the added mass, the phase shift enables some smaller body lengths to have higher damping values per displacement than the longer body lengths (Figure 4.16).

The longer the body, the smaller the effect of lengthening is on the amplitude of the quantity or on the "phase shift" of the behaviour. In general, the values for added mass and damping seem to converge around the length of $20T$, which means that the difference between the values in comparison to $50T$ are negligible. These values can also be assumed to be very close to the 2D-solution.

Something to be noticed are the values of added mass and damping for the two shortest lengths, $0.5T$ and T . The added masses are close to a constant value over the studied range of frequencies and the derivative of the damping term is very small. For both added mass and damping, the peak values of these two shortest lengths are considerably smaller, than those of the longer lengths.

The peak value and the frequency for the peak value are estimated based on the results (Figure 4.13). When these values are plotted as a function of length, Figures 4.14 and 4.15, are obtained. The peak frequency of sway added mass follows a reciprocal curve quite closely. However, this is not so in the case of damping, although a similar pattern can be observed. The noticeable fact in damping, is the value of the peak frequency at the length $10T$, that exceeds the one at $5T$. The actual peak values of sway for added mass and damping behave in a different manner, when compared to one another. For the added mass, a reciprocal function can be neatly fitted to

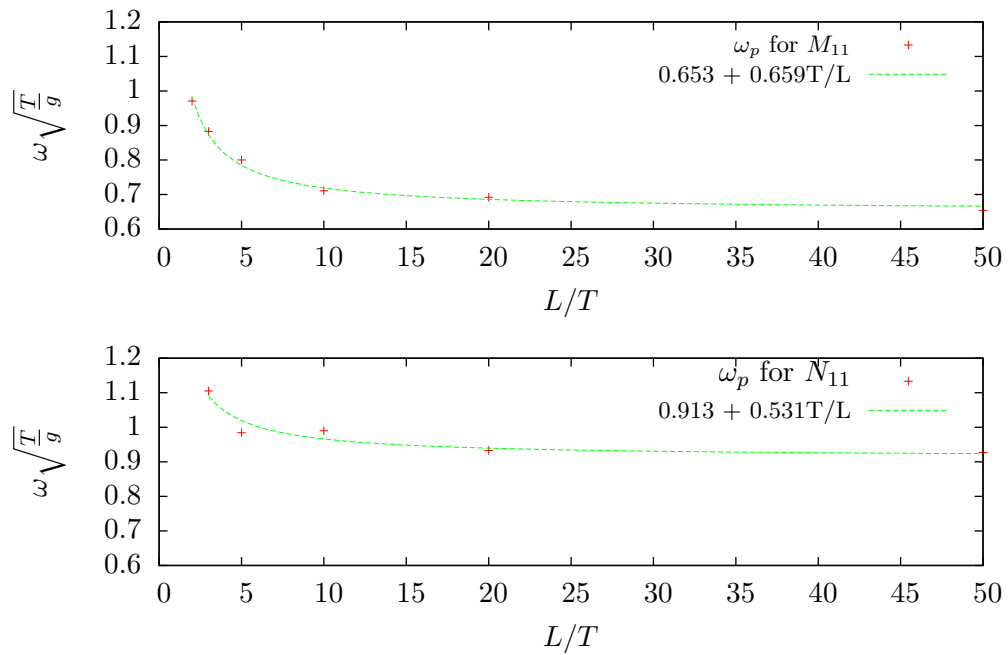


Figure 4.14: Peak value frequencies for sway as a function of length and fitted curves.

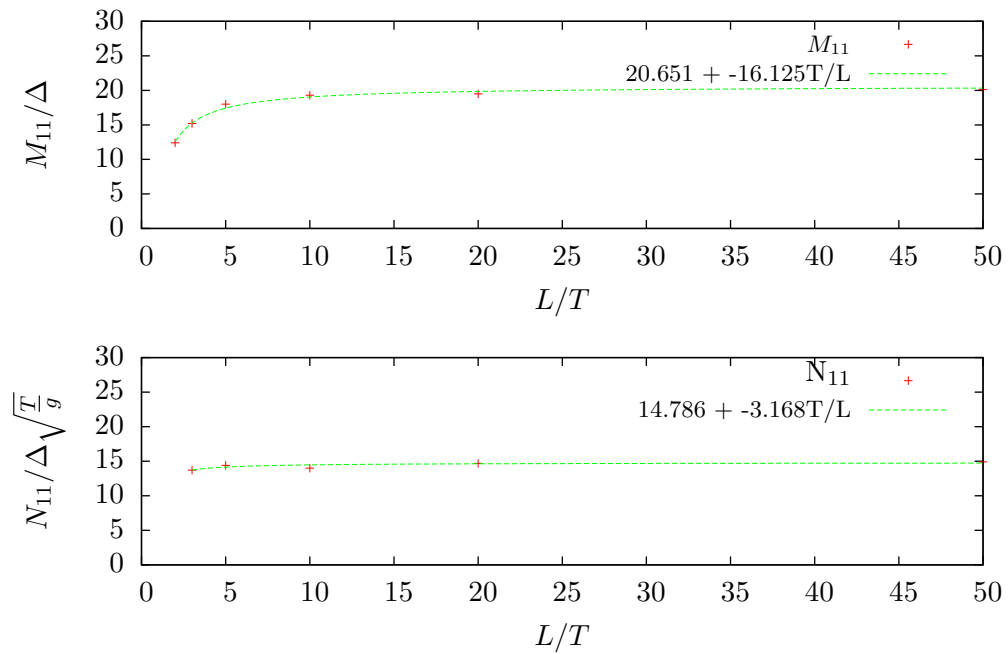


Figure 4.15: Peak values for sway added mass and damping as a function of length and fitted curves.

match the points. However, when the same curve is fitted to damping, it more or less looks like a constant. The behaviour of peak value of damping over the different lengths is quite constant.

When few frequencies are chosen (corresponding to wavelengths $15.7T$, $7.9T$ and $5.2T$), and the values of added mass and damping are observed as a function of length (Figure 4.16), the behaviour can vary relatively much, between those frequencies. At the lowest frequency, both the added mass and the damping increase harmoniously towards the maximum value, which is presumably the 2D solution of the geometry's added mass and damping. When the frequency is increased (i.e. wavelength decreased), the added mass appears to behave in such a way that there is a rapid increase towards the peak value, after which there is a decrease that is followed by a settling towards a constant. Similar behaviour can be found in damping, although the peak effect seems to start later (at a higher frequency) and be smaller (the peak value is not much greater than the value damping is settling to).

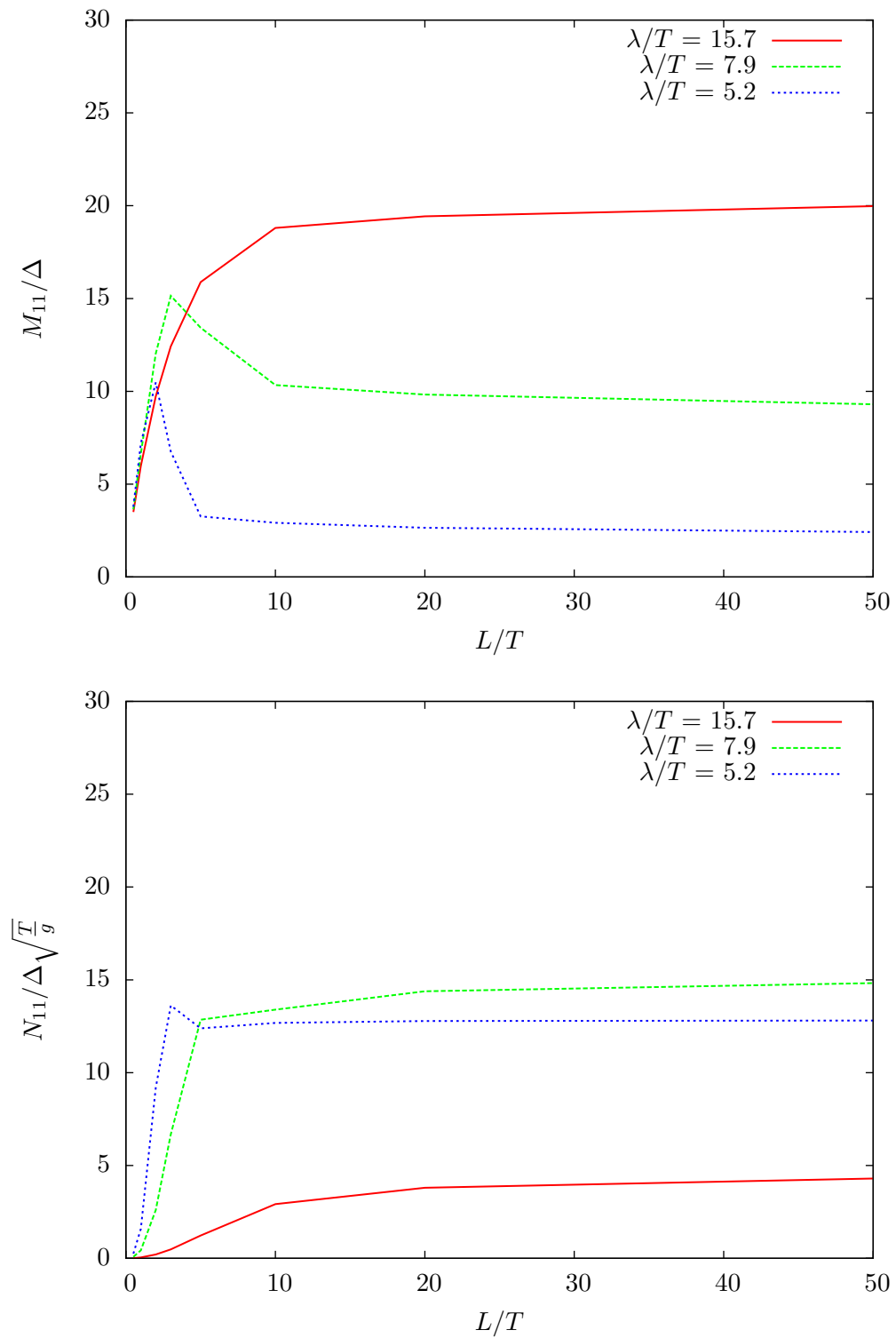


Figure 4.16: Flap sway added mass and damping as a function of the length of the body with three different frequencies

4.3.2 A rolling flap

The results for a rolling flap are presented in this section. An analysis of these results is presented together with the graphs. The roll for the flap takes place around a point at $y = -T$. The B/T ratio of a flap is $1/8$. A Schematic presentation of the situation is represented in Figure 4.17.

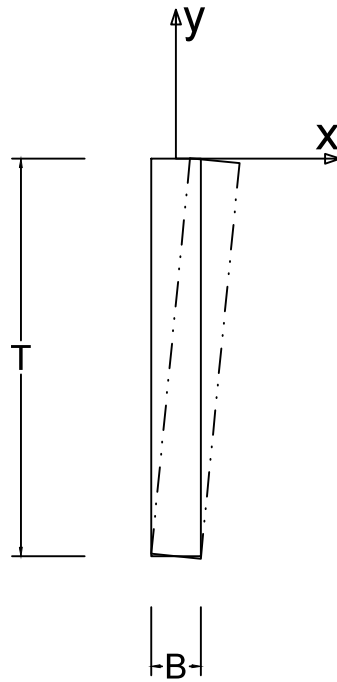


Figure 4.17: A schematic presentation of the rolling flap.

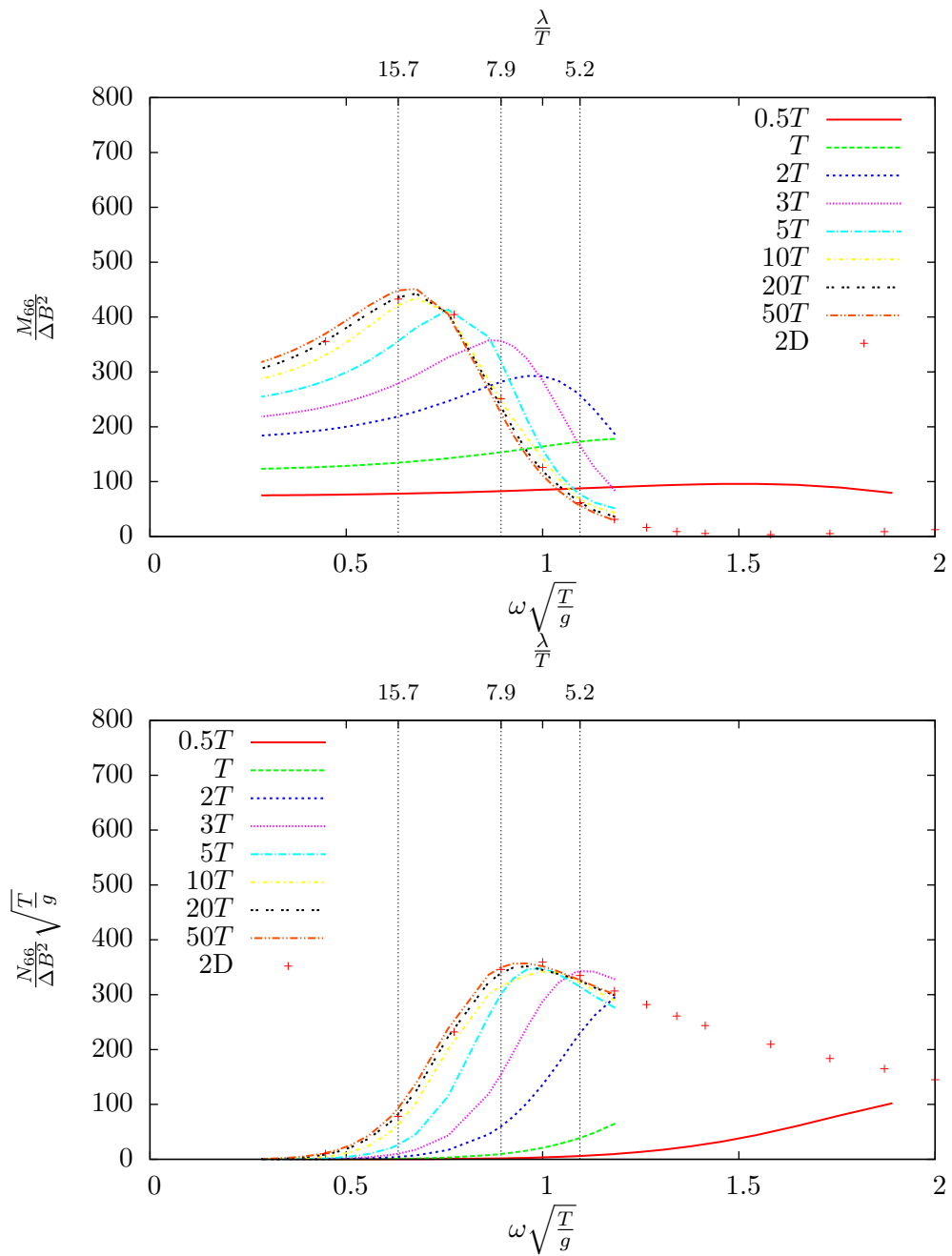


Figure 4.18: Flap roll added mass and damping as a function of the dimensionless frequency with different body lengths. The results are plotted against the analytical 2D-solution for a vertical strip by Mei (1976).

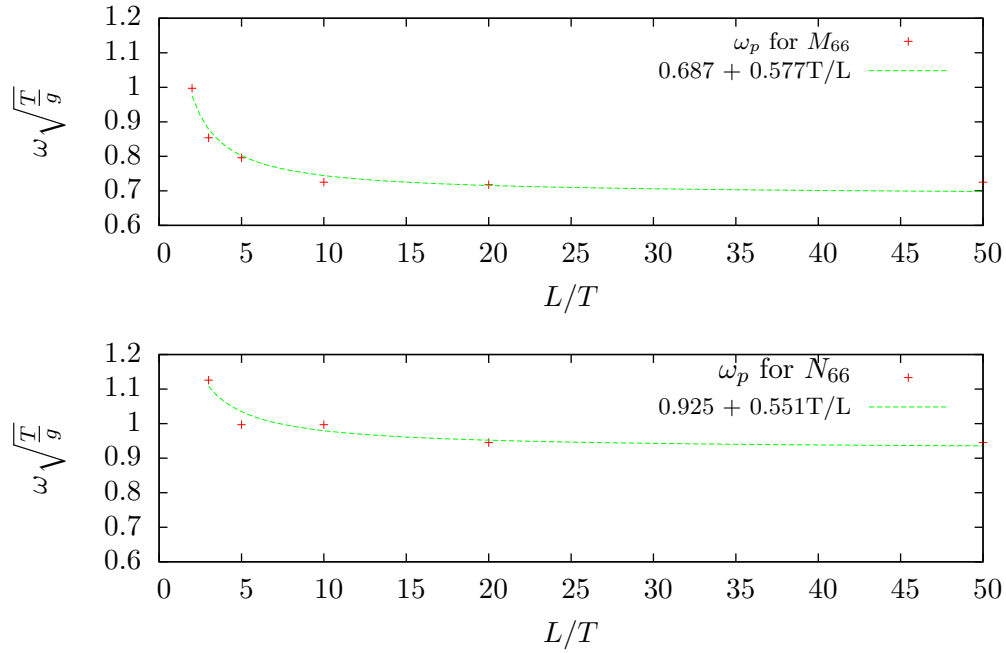


Figure 4.19: Peak value frequencies for roll as a function of length and fitted curves.

The behaviour of added mass and damping of roll as a function of frequency (Figure 4.18) follows closely the behaviour of sway, although the actual values are different. The analytical 2D-solutions obtained from Mei (1976), provide valuable information for the convergence of the results. It indeed is so, that the longest bodies have added mass and damping very close to the 2D solution over the whole studied bandwidth. The reason for some discrepancy between the added mass and damping of the longest bodies and the 2D-solution is probably the fact that the 2D solution is computed for a vertical strip, which has a zero thickness (but is made dimensional for the purposes of comparison), whereas the thickness of the modelled flap is $T/8$.

The peak values as a function of the body length (Figure 4.20) and their frequencies (Figure 4.19) appear similar, when compared to the values for sway. The actual peak values have different values than those for the sway, naturally. As in the case of sway damping, so it is for roll damping: the values are very close to constant, regardless of the length.

The added mass and damping as a function of length (Figure 4.21) for roll are very similar to the sway behaviour of the flap.

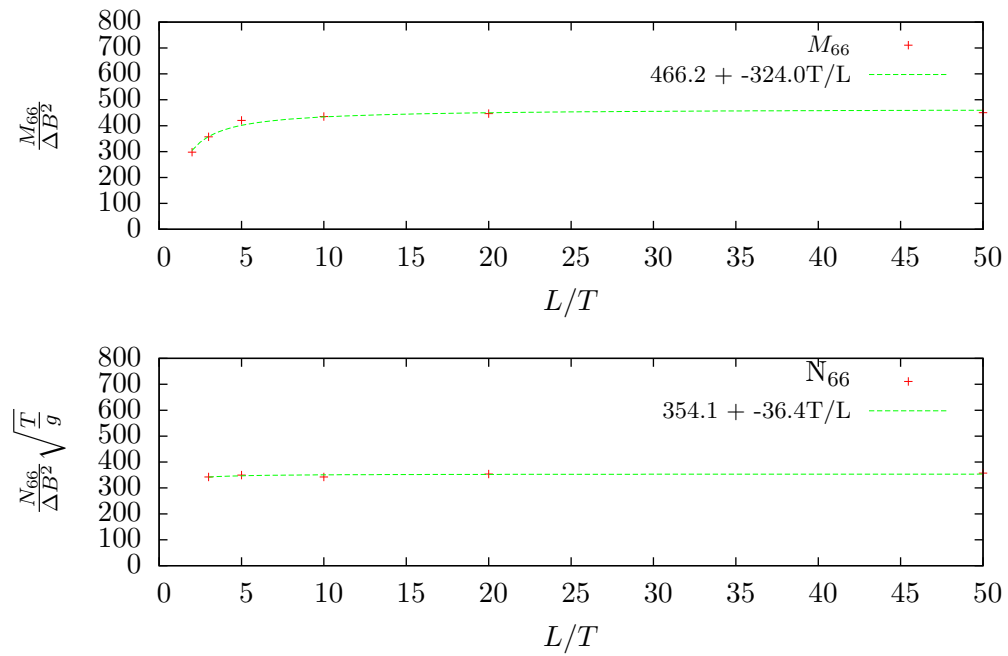


Figure 4.20: Peak values for roll added mass and damping as a function of length and fitted curves.

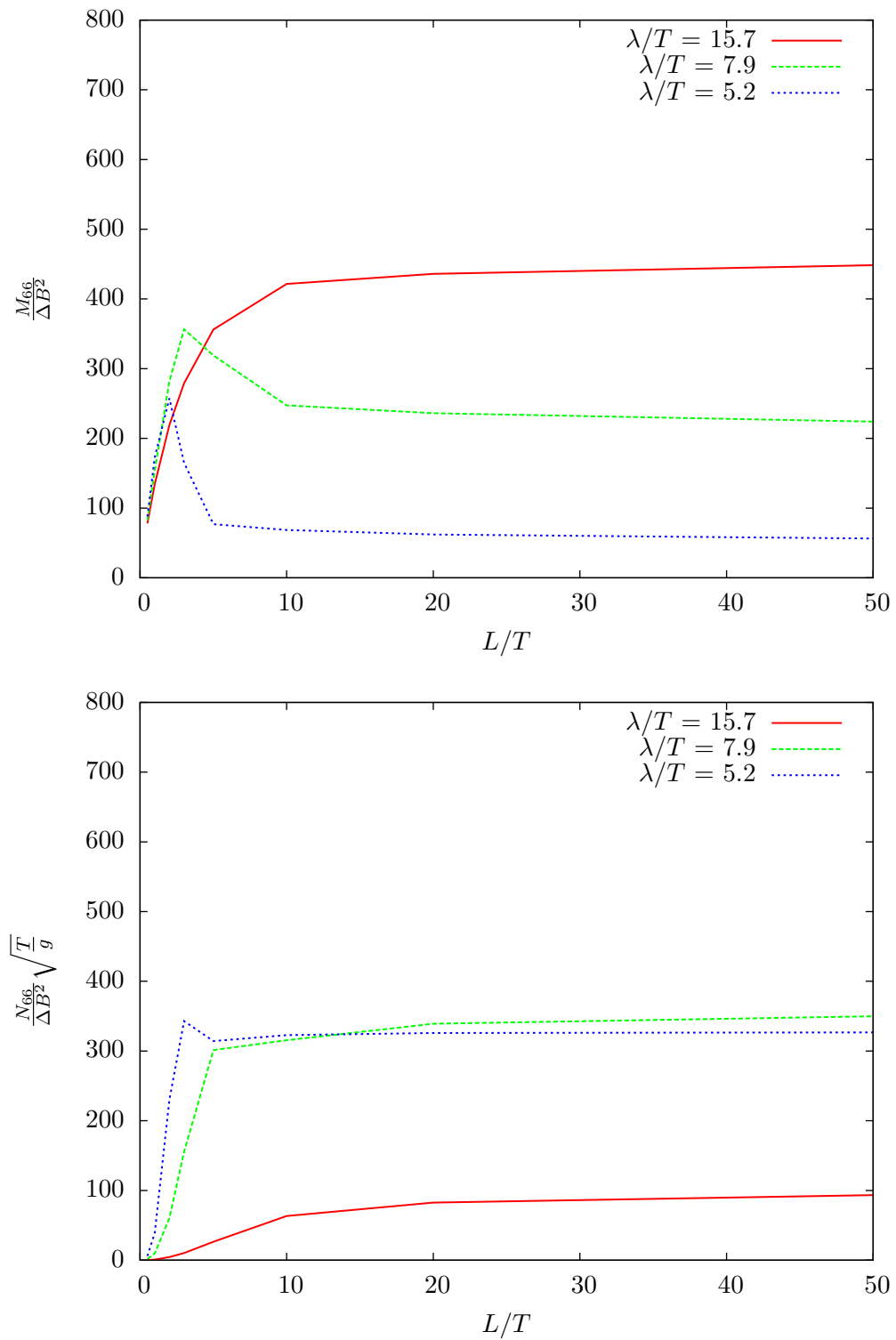


Figure 4.21: Flap roll added mass and damping as a function of the length of the body with three different frequencies

4.3.3 A swaying barge

In this section, the results for a swaying rectangular barge are presented. An analysis of these results is presented together with the graphs. The B/T ratio of the rectangular barge is 2. A schematic presentation of the situation is seen in Figure 4.22.

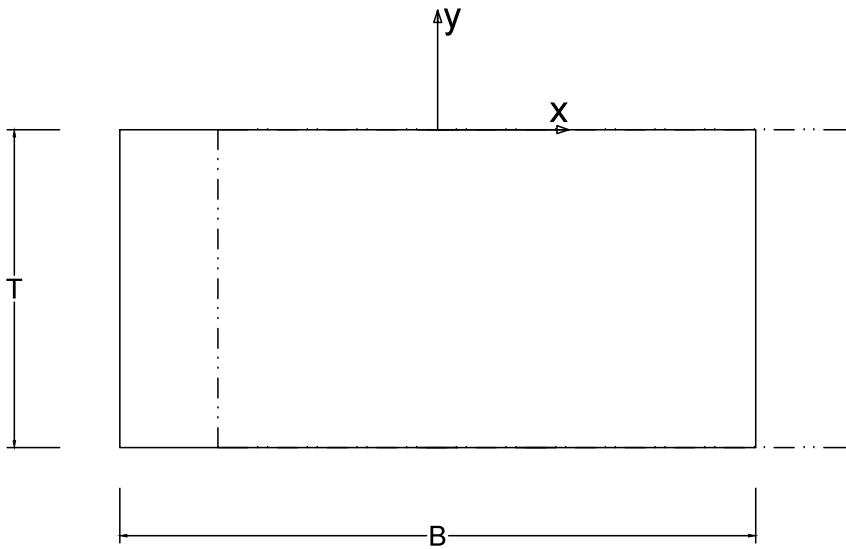


Figure 4.22: A schematic presentation of the swaying rectangular barge.

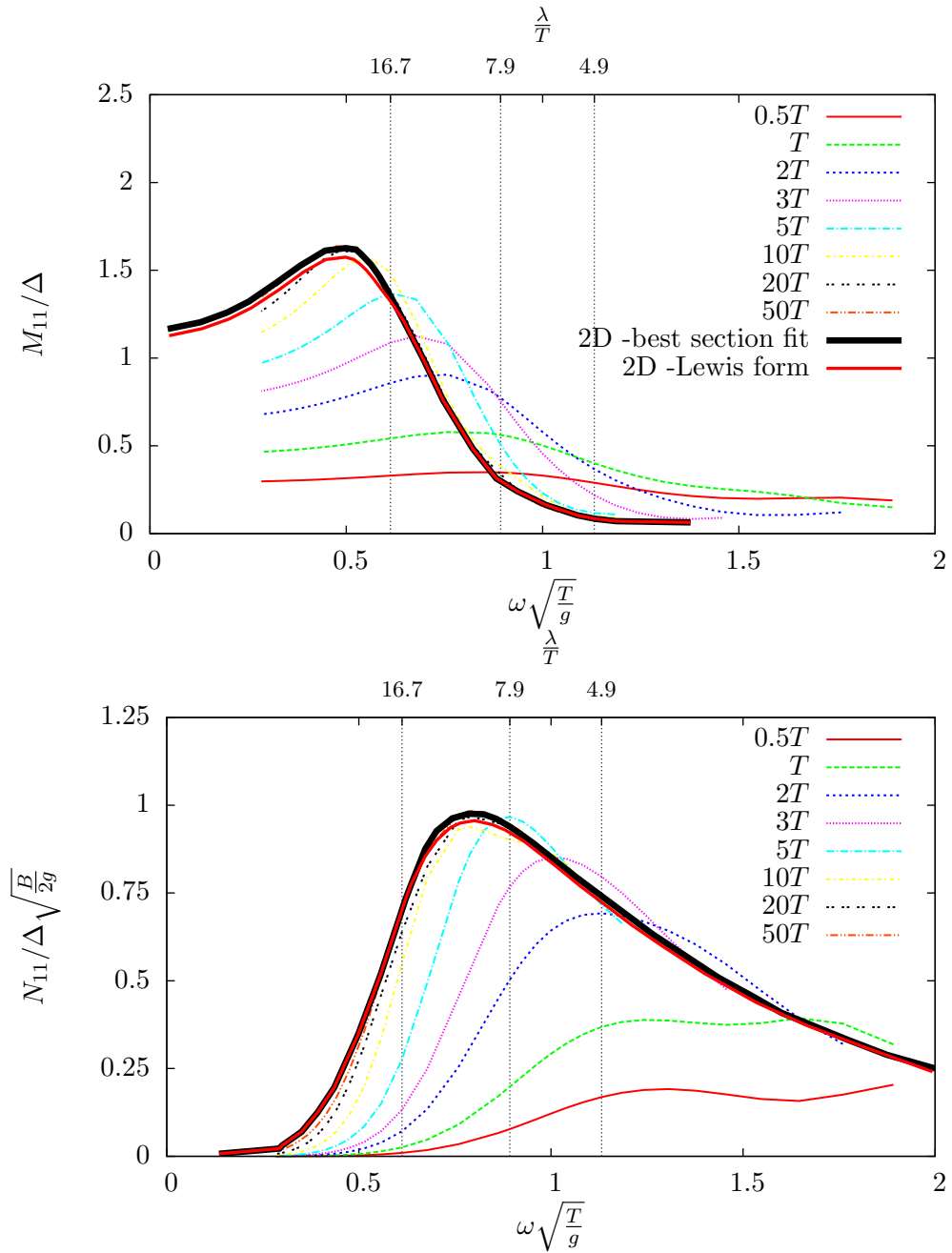


Figure 4.23: Rectangular barge sway added mass and damping as a function of the dimensionless frequency with different body lengths. Results are plotted against the 2D results by Vugts (1968).

The 2D-solutions presented by Vugts (1968) correspond very closely to the results obtained by Garrison's Panel Method, regarding the barge with the length of $50T$ (Figure 4.23). The nature of the results is similar to the ones with the flap. In the 2D-solution of added mass, there is first an increasing trend up until the dimensionless frequency of 0.5 after which there begins a decrease, that remains linear for some time. Slowly the derivative begins to approach zero but does not reach it. As it happened with the flap damping, so does it happen with the damping of the rectangular barge. The values begin from zero, but reach their peak value rapidly. The peak value of damping is reached when the second derivative of the decreasing added mass shifts from negative to positive (as it did with the flap). The 2D-damping decreases slowly and more or less constantly from its peak value to one fourth of this. At this point the dimensionless frequency reaches the value of 2.0. The same two characteristics that were visible in the case of the flap, also apply to the behaviour of the rectangular barge in sway when the length decreases. There is a decrease in the value of added mass and damping per displacement when the length is decreased and when there is a "phase shift" of the characteristic behaviour towards higher frequencies.

The noticeable difference between the barge and the flap is the fact that the characteristic behaviour typical to both geometries begin earlier with the barge than it does with the flap. So changing the geometry from a flap to a barge causes a "phase shift" towards lower frequencies. This also reveals behaviour at the higher frequencies and shorter body lengths that was not visible in the case of the flap, especially in the case of damping. Whether this phenomena would occur in the case of the flap, is unclear and would require further studies with higher frequencies.

The peak value frequencies of added mass and damping as a function of length (Figure 4.24) follow the form, which they did with the flap. A reciprocal function can be fitted to follow the peak points obtained from the computations. What is noticeable though, is the fact that for flap sway damping, the peak frequency of $10T$ was higher than the one for $5T$. However, this is not the case anymore regarding the rectangular barge.

When observing the actual peak values of the added mass and damping (Figure 4.25), the fitted curves fit neatly. With the flap, the damping was linear, but with the rectangular barge a reciprocal behaviour can be seen. It is possible that the behaviour would eventually also be reciprocal with the flap. However, to find out whether this is the case, it would require the expansion of the computations to higher frequencies. However, this is not included in the scope of this thesis.

The sway added mass and damping as a function of length (Figure 4.26) have the same characteristics as the quantities for the flap. The chosen wavelengths are very close to those chosen for the flap, but because of the properties of the geometry, the different characteristics of the behaviour occur at different frequencies. This signifies that for the three chosen fre-

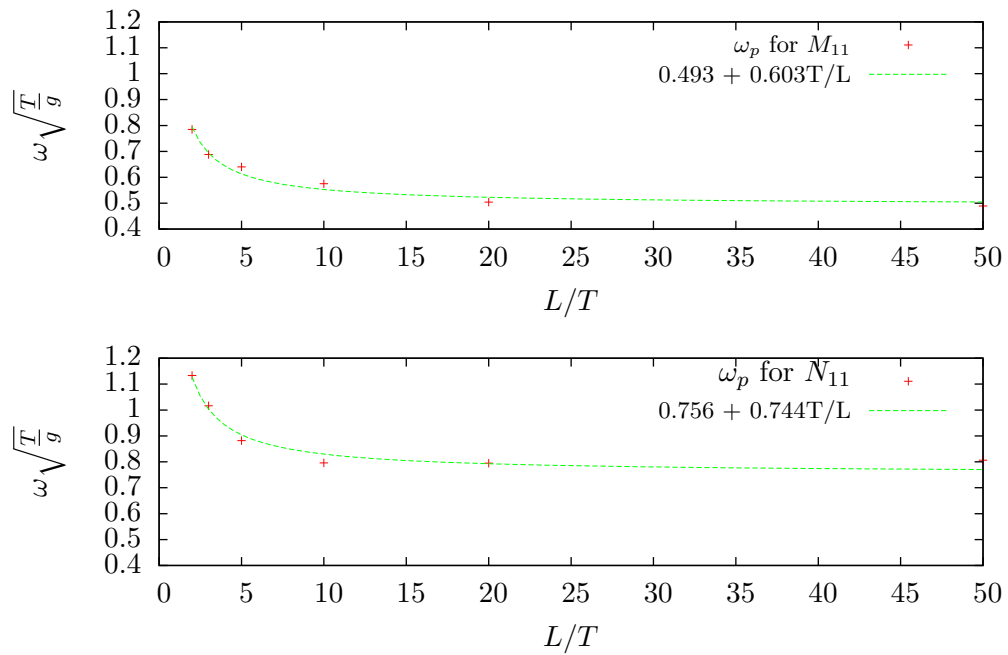


Figure 4.24: Rectangular barge peak value frequencies for sway as a function of length and fitted curves.

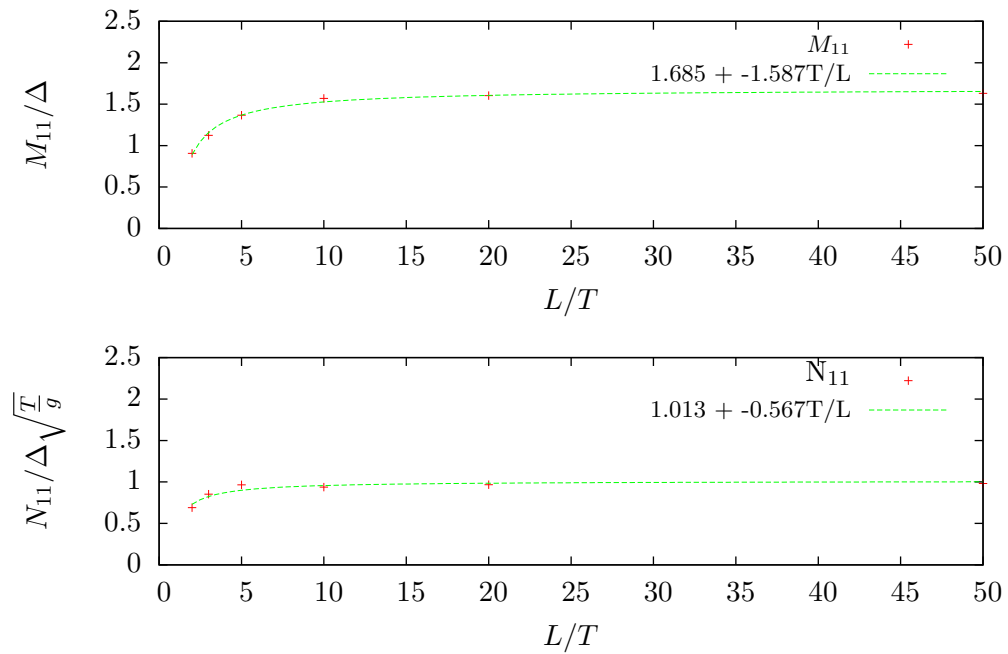


Figure 4.25: Rectangular barge peak values for sway as a function of length and fitted curves.

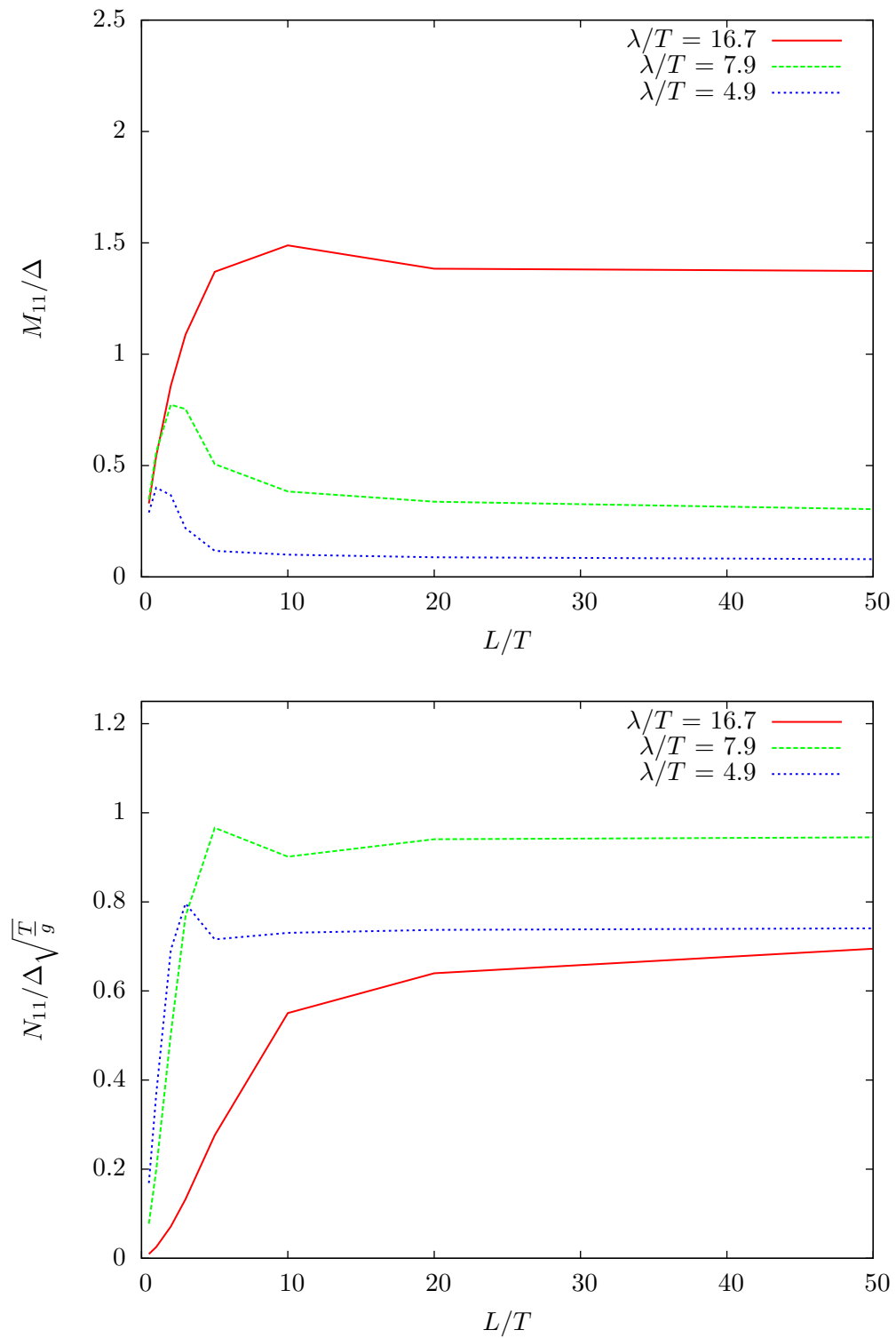


Figure 4.26: Rectangular barge sway added mass and damping as a function of the length of the body. Different lines correspond to different $\omega\sqrt{T/g}$ values.

quencies, the figures do tend to appear different, than those of the flap. For the added mass of sway, all of the chosen frequencies show similar behaviour in comparison to each other. A peak value is obtained, after which there is a decrease towards a constant, which is the 2D solution. The lowest frequency has clearly the highest values of added mass. With damping, the lowest frequency gradually increases to the 2D solution. The middle frequency has a peak, a dip, and then a gradual increase to the constant value, when the length is increased. The highest frequency behaves so, that it rapidly obtains its peak value at $3T$ and then rapidly settles to a constant value at $5T$.

4.3.4 A rolling barge

In this section, the results for a rolling rectangular barge are presented. An analysis of these results is presented together with the graphs. Roll for the barge takes place around the z -axis. A schematic presentation of the situation is represented in Figure 4.27.

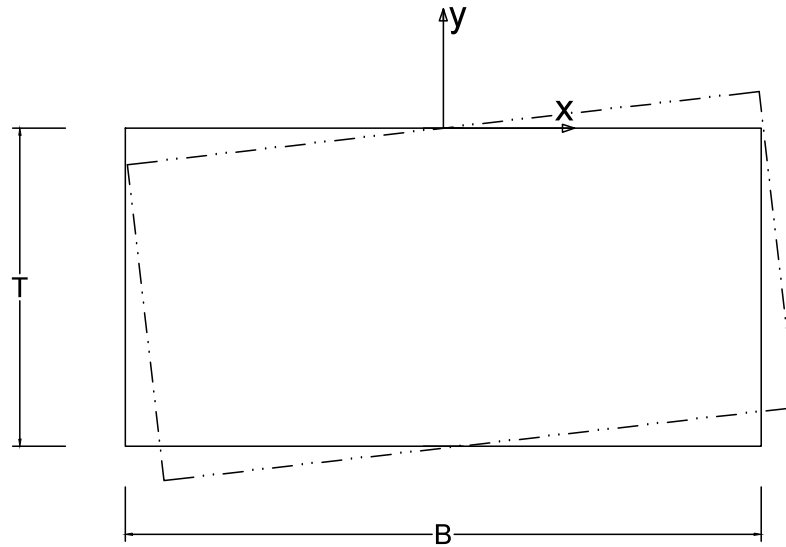


Figure 4.27: A schematic presentation of the rolling rectangular barge.

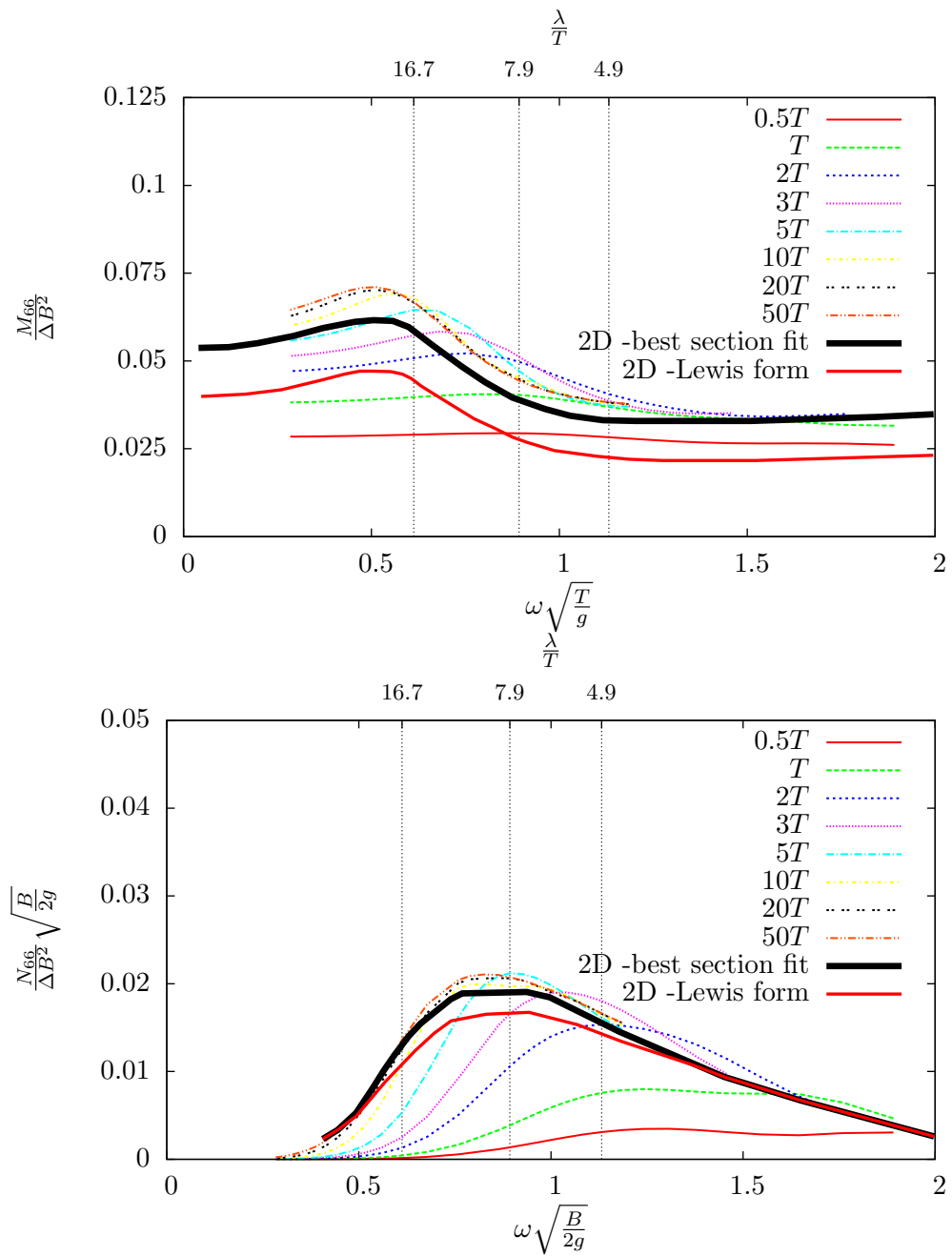


Figure 4.28: Rectangular barge roll added mass and damping as a function of the dimensionless frequency with different body lengths. Results are plotted against the 2D-results by Vugts (1968)

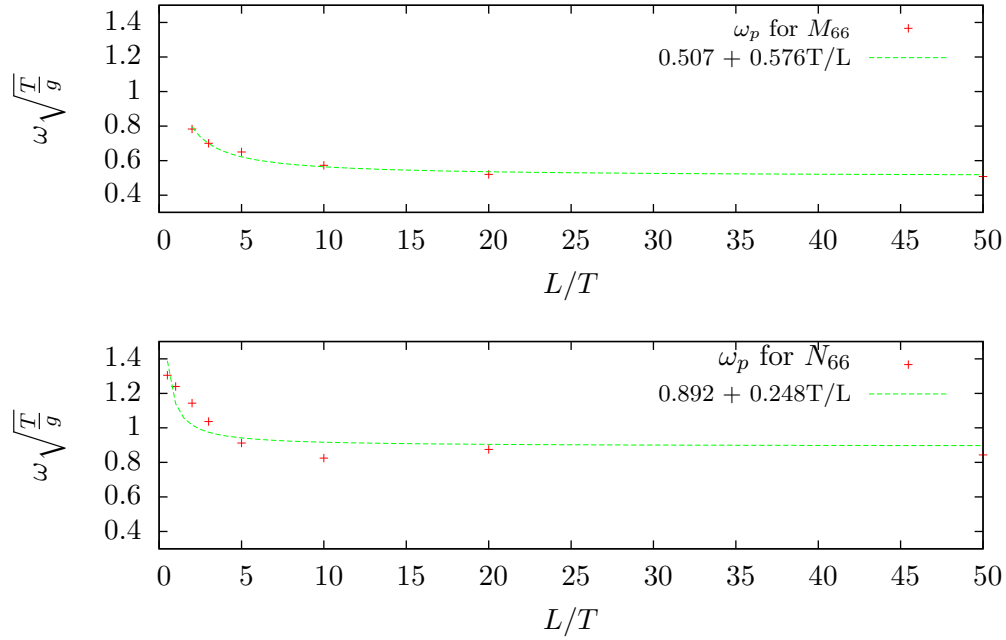


Figure 4.29: Rectangular barge peak value frequencies for roll as a function of length and fitted curves.

It is important to note that with the rectangular barge, the point of origin is at the waterlevel $y=0$, whereas with the flap it is at $y=-T$.

The roll behaviour of the rectangular barge as a function of the frequency (Figure 4.28) appears analogous with the sway behaviour. The noticeable fact is the discrepancy in 2D results in comparison to each other and also with the longest bodies of the barge. There are two 2D-results and neither corresponds to the 3D-results. However, it seems that at all of the frequencies, the differences between the three different lines (two 2D-results, and the result for barge having the length of $50T$) remain constant.

The peak value frequency for added mass as a function of length (Figure 4.29), follows the reciprocal representation quite neatly. However, this is not the case with damping. With damping the peak value frequency drops linearly when the length is increased from $0.5T$ to $5T$, after which it obtains somewhat of a constant value, independent from the length of the geometry. The behaviour of the actual peak values as a function of length (Figure 4.30), follow a reciprocal representation with the added mass and somewhat with the damping.

The added mass and damping values of roll as a function of length (Figure 4.31) of the rectangular barge are very similar to those values of sway. The only noticeable difference is the magnitude of the values.

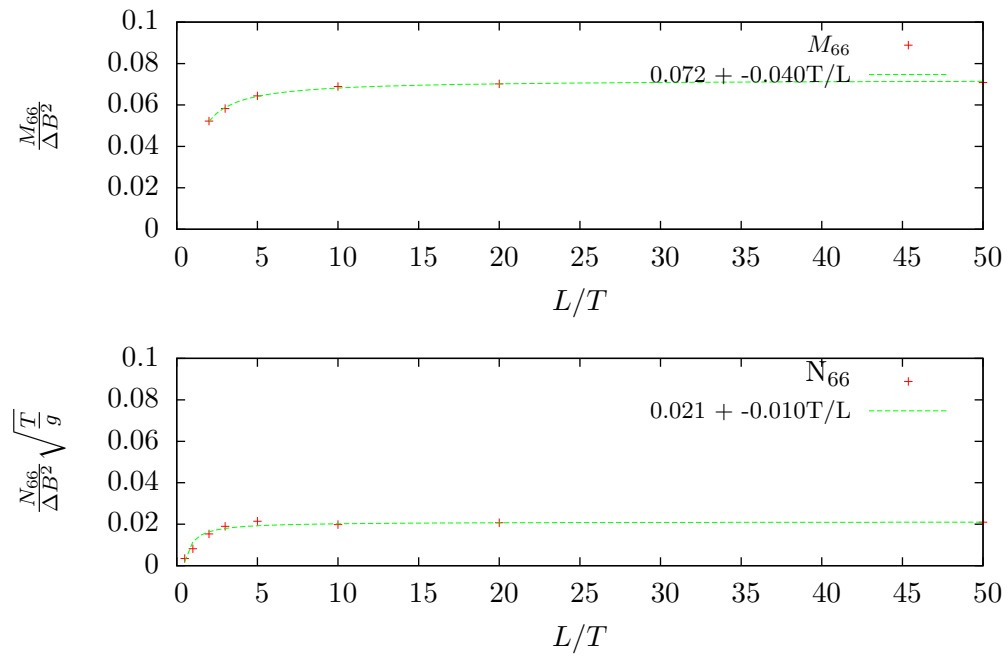


Figure 4.30: Rectangular barge peak values for roll as a function of length and fitted curves.

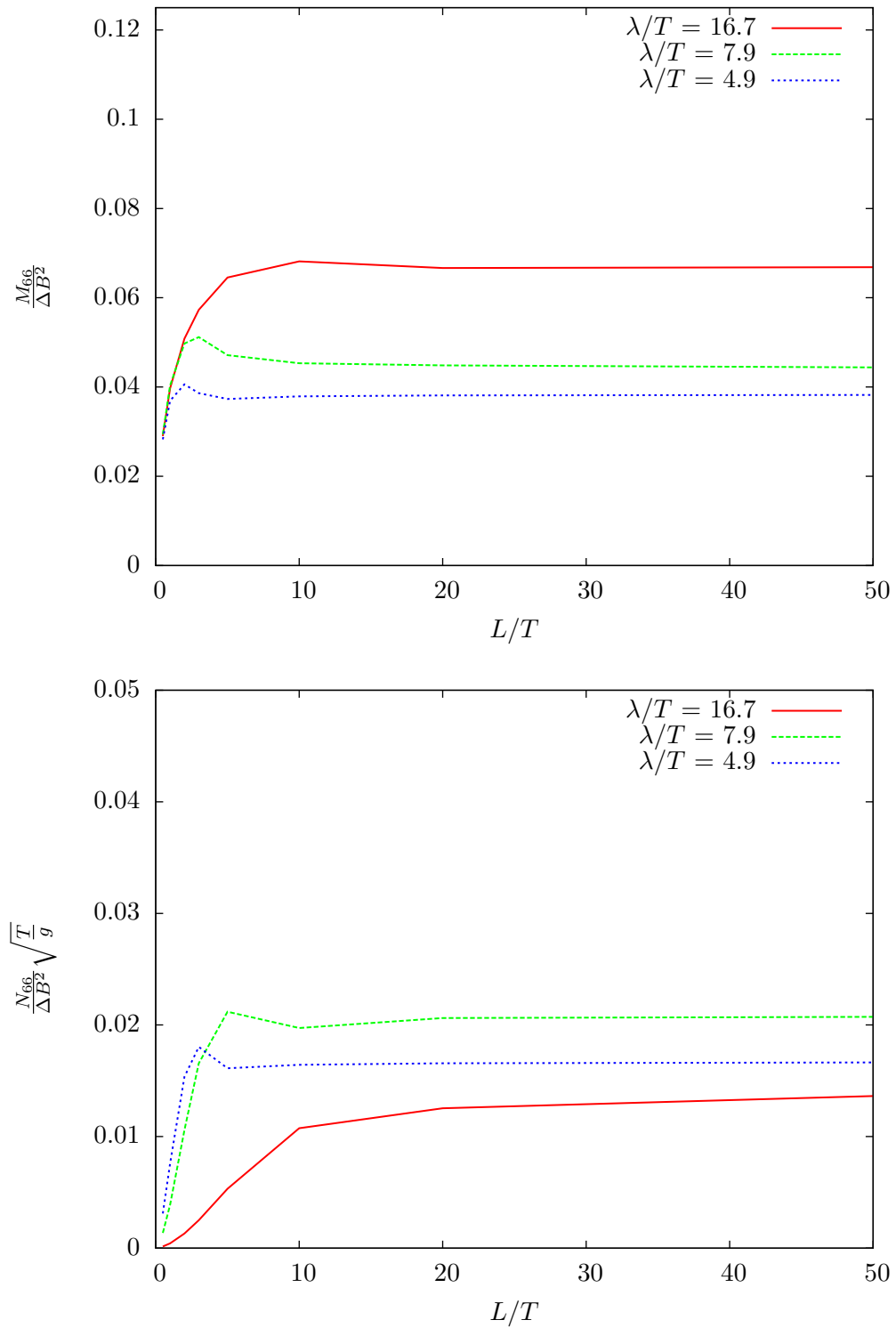


Figure 4.31: Rectangular barge roll added mass and damping as a function of the length of the body. Different lines correspond to different $\omega\sqrt{\frac{T}{g}}$ values.

4.3.5 A heaving barge

In this section, the results for the heaving rectangular barge are presented. An analysis of these results is presented together with the graphs. A schematic presentation of the situation is seen in Figure 4.32.

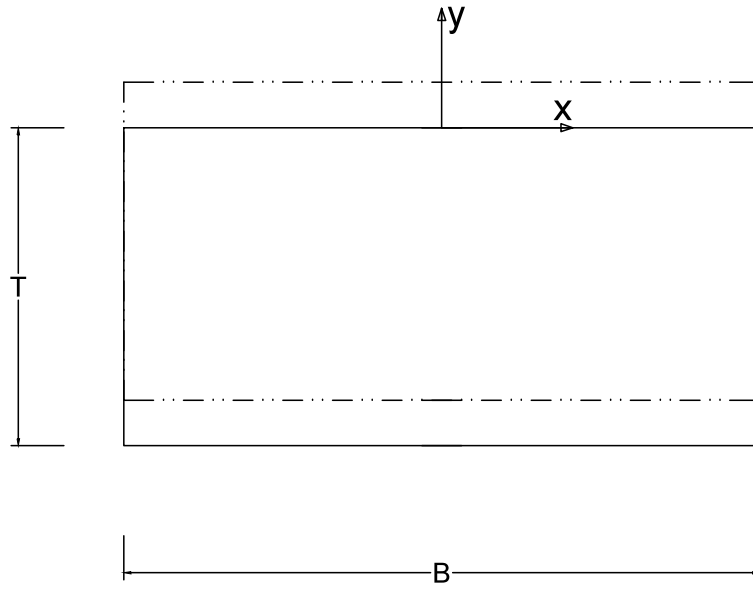


Figure 4.32: A schematic presentation of the heaving rectangular barge.

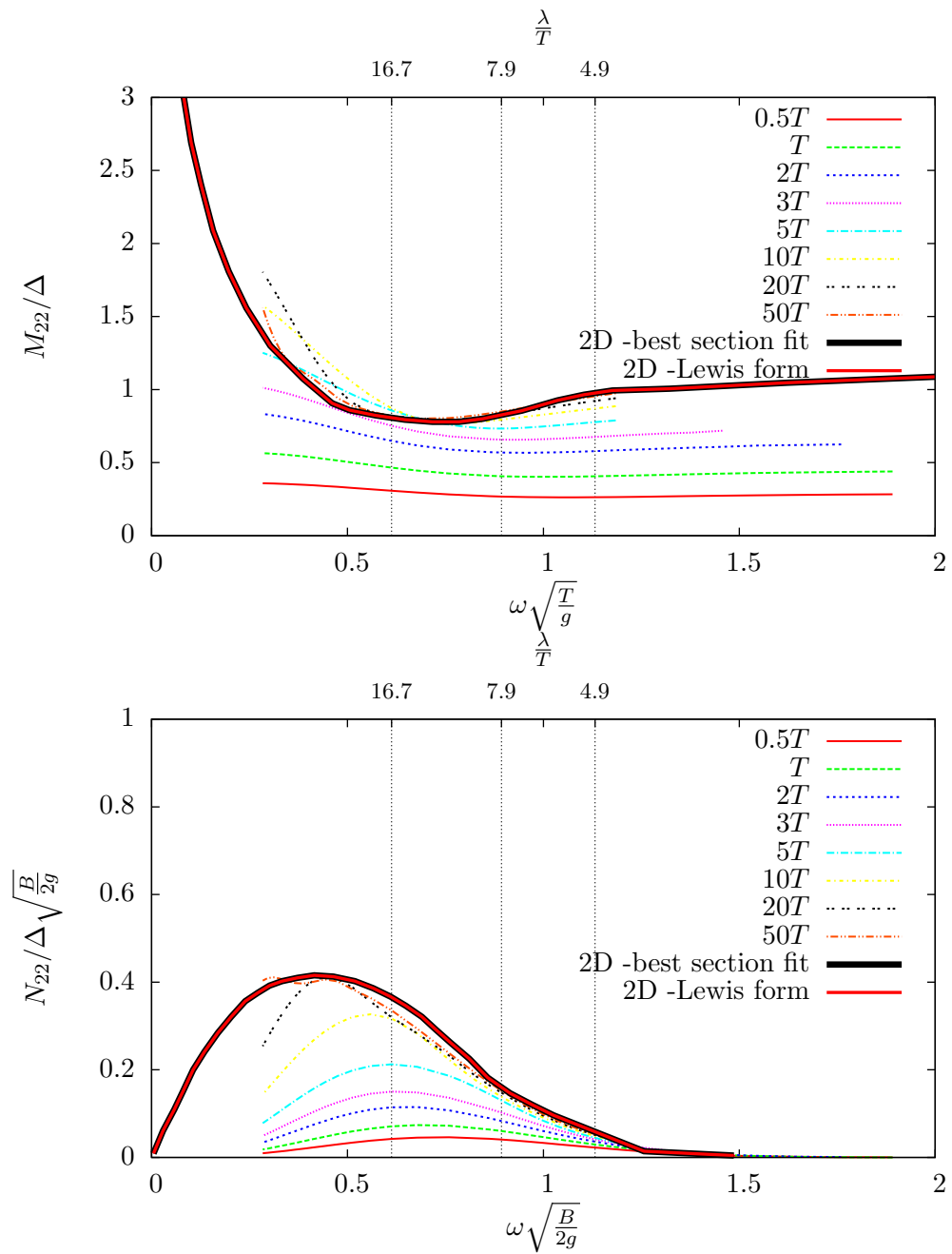


Figure 4.33: A rectangular barge heave added mass and damping as a function of the dimensionless frequency with different body lengths. The results are plotted against the 2D results obtained by Vugts (1968).

The results for added mass and damping of the heave of the rectangular barge are presented as a function of the dimensionless frequency (Figure 4.33) as well as a function of the body length with three different frequencies (Figure 4.34).

The 2D solutions for heave, appear to accurately match each other. What takes place in the 2D-case when the frequency is increased from zero, is that the value of added mass decreases from infinity and reaches its minimum value (0.9 of its mass) somewhere around 0.75 of the dimensionless frequency. The added mass increases again slightly, after which it appears to obtain a linear increase up until the end (of the range of study). With damping, the 2D solution increases from zero and finds a maximum value at around 0.45 of the dimensionless frequency. It decreases in a similar manner as it grew. However, soon the decrease begins to slightly decelerate. The damping finally settles to zero, around 1.5 of the dimensionless frequency.

It appears that the three-dimensional behaviour of heave also has the two elements in it, which were characteristic to sway and roll. These are the decrease of their values and the "phase shift" towards higher frequencies. However, there is something else also visible in this heave behaviour and it comes out in the case of added mass and especially at the lowest values of the chosen frequencies. Firstly, the added mass of $50T$ is not exactly on top of the 2D curve. Especially at the lowest frequency, there is a clear difference between it and the 2D-value. Secondly, when the dimensionless frequency is less than 0.7 all the values of added mass with lengths above $5T$, top the 2D-values. This takes place in a way that does not look systematic. The damping of heave at these frequencies behaves in a systematic way. Although the longest bodies with lengths of $10T$, $20T$ and $50T$ appear to have unexpectedly high values of damping. There is also a peculiar "dip" with the length of $50T$ at around 0.4 of the dimensionless frequency. The remaining values of heave damping with the different lengths behave in an expected way, compared to each other and the 2D solutions.

The added mass of heave as a function of the body length (Figure 4.34) appear to behave in quite a similar manner for all the chosen frequencies. The values are almost the same for all three of the frequencies over the lengths. The two higher frequencies behave similarly, and finally differ only slightly in their values. However, for the lowest frequency, there is a peak value that is reached somewhere between $5T$ and $10T$. After this, there is a slight decrease in the value before a constant is reached. For damping the nature is the same for all of the three frequencies. The lower the frequency, the higher the damping. The damping increases as a function of frequency until it reaches its maximum and then remains constant. However, this constant is not the 2D solution at the lowest frequency, as can be observed when compared to Figure 4.33.

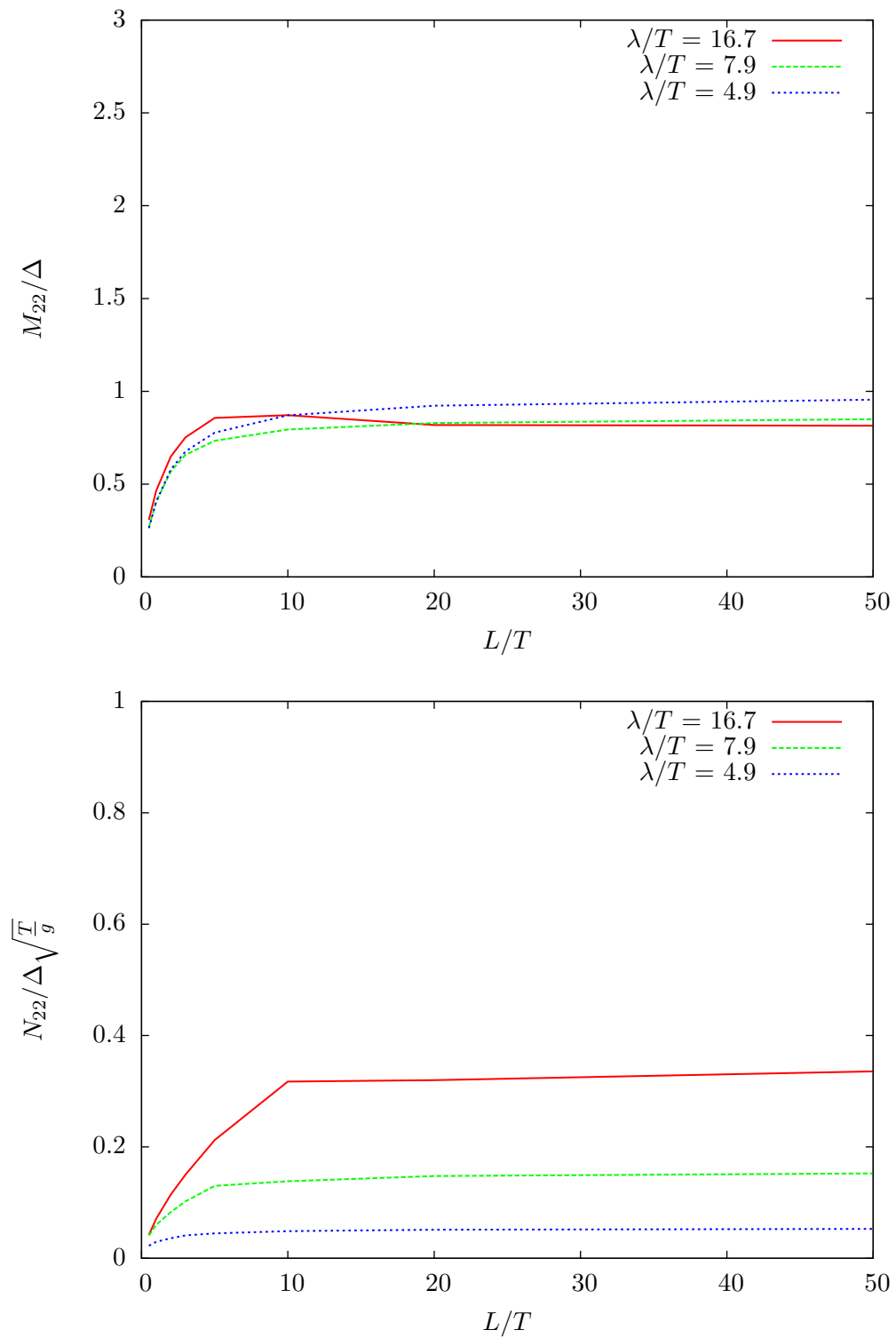


Figure 4.34: A rectangular barge heave added mass and damping as a function of the length of the body. The different lines correspond to different $\omega\sqrt{T/g}$ values.

4.3.6 The radiation pressures

Garrison's program provides pressures, and their phase on each panel (which can be presented as added mass and damping contributions). These quantities provide information related to the research question - the effect of three-dimensionality on radiation forces, which is why they are presented in this study. Due to the quantity of the graphs, it is seen wise to present the added mass and damping distributions in the Appendix A.

For the sake of brevity, the distributions of added mass and damping will be presented only to the sway of the flap. Sway is the only quantity that is comparable between the two geometries. It is believed that the study of this one geometry in the light of radiation pressures will provide a desirable amount of additional understanding, regarding the research question. The chosen frequencies for the radiation pressure distribution figures are those already used in this thesis. The corresponding wavelengths to those frequencies are $15.7T$, $7.9T$ and $5.2T$.

When the results for the radiation pressures are studied, there are a few observations that can be made. They are enumerated here, after which a short paragraph is written about each of them.

1. The behaviour of added mass and damping distribution at the end of the geometry with a chosen frequency is almost identical with body-lengths, that are equal or greater than $5T$.
2. The wavelengths can be deduced from the results when looking at the radiation pressure distributions.
3. The damping values are small for short body-lengths, even more so when the frequency is small.
4. Added mass distribution with the longest bodies at the lowest frequency is very uniform.
5. The higher the frequency, the closer is the damping distribution concentration to the water level.
6. When the frequency is high, the added mass distribution is concentrated at the bottom of the geometry with longer body lengths.

It appears that when the length of the body is higher than $5T$, the pressure distribution at the end of the geometry is independent of the body length, for both added mass and damping. This is the case, even if the pressure distribution elsewhere around the body is different, between different lengths (see e.g. added mass at wavelength $\lambda = 7.9T$ with lengths $5T$ and $10T$ in Figure A.4).

At the observed frequencies and body lengths, many of the geometries are shorter than the wavelength in question. However, this is not always the

case. When the results are observed, there is a pressure distribution, which clearly reveals the wavelength of the frequency in question.

The damping values are small at low frequencies and especially with short lengths. This is intuitive for two reasons. The low frequency movement does not generate waves and the "leakage close to the edges" is dominant with short lengths. The latter sentence means that a bulk of the water particle movement goes to circulation around the body, which contributes to added mass, not to damping.

The added mass distribution at the lowest frequency is very uniform over the body length. It is especially so at the longest body-lengths. This is somewhat intuitive, since the damping is small and therefore, waves do not create much variation in the distribution. At this frequency a close approximation regarding the added mass distribution in 2D in the vertical direction can be made.

A general observation that can be made in the case of damping is that the higher the frequency, the higher (vertically) is the "weighted center of gravity" of the concentration. Also, the higher the frequency, the thinner the concentration. This is perhaps clearest if the damping is compared at wavelengths $\lambda = 7.9T$ and $\lambda = 5.2T$ (Figures A.3 and A.5).

Characteristics in the added mass that are different compared to two of the lower frequencies is that when the frequency is corresponding to $\lambda = 5.2T$, the "weighed center of gravity" at the longest lengths ($5T$ upwards) is clearly below the horizontal center line of the body. Furthermore, the distribution has parts where the added mass per unit area is zero, or even negative. For these characteristics to occur, two conditions seem to be fulfilled: First, the characteristic phase of the added mass is where the highest decrease has already been reached (see Figure 4.13). Second, the body length equals, or is higher than the oscillation wavelength.

Chapter 5

Discussion

The aim of this thesis was to find out the effect of three-dimensionality on radiation forces with surface piercing bodies. The computations were performed with the help of a panel-method developed by Garrison (1974). In addition to answering the research question it was hoped that the applicability and perhaps also the validity of Garrison's program would be established, during this process. A general theory behind linear waves, Potential Flow, and Panel Methods was presented at the start of this thesis. After this, a presentation of the studied cases was made. The chosen cases were a circular cylinder (Garrison, 1975, 1978), to verify the computation results, as well as two other cross sections for the study of the effect of three-dimensionality on the radiation forces. The two latter chosen cross-sections were a flap with an aspect ratio (B/T) of $1/8$, and a barge with an aspect ratio of $2/1$. The lengths of these cross sections spanned from $0.5T$ to $50T$. It was important to make sure that the different panel arrangements did not have an unfavourable effect on the results, and therefore a panel resolution study was performed for both geometries, by a chosen method. The procedure of choosing proper grid resolutions was presented after the chosen cases, and the results for this resolution-study were presented in the Results (Chapter 4). The simulations with the Garrison's program were performed for the two cross-sections and all of their lengths for oscillation periods between 3 and 20 seconds. The results for added mass and damping were presented as a function of frequency for all body lengths and as a function of length for three chosen frequencies. The peak values of added mass and damping as well as their frequencies were also plotted to reveal their behaviour as a function of the body lengths. The modes of motion for the flap were sway and roll and for the barge sway, roll and heave. The roll for flap was computed around the point at depth T and for the barge around the point at water-level. In addition to this, the distribution of added mass and damping (the radiation pressures) on the flap in sway were presented. The results are discussed in this Chapter. The objective is to pinpoint the relevant findings and to draw conclusions.

In the light of the results, it is clear that the radiation forces have a characteristic behaviour pattern, which is independent of the length of the body. This characteristic behaviour is very clear in the 2D case (or with the longest lengths). The variation of the length of the body has a twofold effect on this characteristic behaviour. First, when the body is shortened from the infinite length (2D-case), the curves of added mass and damping shift to higher frequencies. Second, the shortening causes the values to drop. This value drop is especially clear with added mass, but no so evident with the damping.

When the results (only sway and roll) are observed from the point of view of peak values and their frequencies, it is perhaps surprising to notice that especially in the case of added mass, these values follow reciprocal functions very faithfully. This is not so evident with added damping, although such trend might be observable.

Plotting the added mass and damping as a function of length is quite relevant from the point of view of the research question. However, it should be noted that these graphs alone would not provide the kind of information necessary to explain the possible reasons behind the behaviour. When it is understood that there are different phases in the characteristic behaviour of the forces, the results become comprehensible. If the behaviour is in the same phase with all of the lengths (Figure 4.16, wavelength 15.7T) then the behaviour is predictable as a function of length, but if the behaviour is in a different phase with varying lengths, then different kind of behaviour can occur (Figure 4.16, wavelength 5.2T). If then one was asked a question: How do added mass and damping behave as a function of length? The answer would be: It depends on the frequency.

The radiation pressure distribution (Appendix A) sheds light on the results discussed earlier. When all the lengths are in the so-called first phase of the characteristic behaviour the effect of shortening of the body causes the added mass and damping to drop in a predictable manner. This predictability can also be observed in the radiation force distribution over the whole span of lengths with the lowest frequency (Figures A.1 and A.2). When some of the lengths have passed the first phase of characteristic behaviour, it can be seen that the pressure distribution over the whole body length can be of very different nature between different lengths. These variations appear to be more pronounced with added mass than damping.

This study reveals two important things. First, when the body is lengthened, a shift occurs in the frequency domain of the characteristic behaviour with both added mass and damping towards lower frequencies. Second, the peak and average values of the quantities increase (up until a certain point) when the length is increased. What could be the possible reasons for such phenomena?

When a body is very *short*, the induced force can be very small, because the particles 'have time' to go around the structure (e.g. A.2), instead of

decelerating in relation to the body motion. It is intuitive then, that the shorter the body length, the greater is the effect of the end of the structure (decreasing the total force). The *shortness* of a body length needs to be understood in the light of the frequency.

Perhaps it can be assumed that the reason for the characteristic behaviour's shift in the frequency domain is the following: The effect of lengthening causes the water particles to become 'slower', in a horizontal direction in comparison to the body length. The water does not have time to go around the body as well, as it does with a shorter body. In other words, for water particles the lengthening of a body is like increasing the frequency of motion. This lengthening of the body then, causes a 'jump backwards' in the characteristic behaviour (Figure 4.18), that is visible in both of the studied geometries.

With the added mass and damping of heave of the barge, although the effects of the shift in frequency domain and average value change were observable, the convergence of the radiation terms towards the 3D -solution did not take place as it did for sway and roll. This is perhaps due to the nature of the added mass of heave, where in the 2D case the values approach infinity when the frequency approaches zero.

In the light of the results, the study of the effect of three-dimensionality on radiation forces with surface piercing bodies can be held successful. It can be observed that the main characteristics of the effect were revealed. This research proved that Garrisons program is able to provide results whose reliability can be held at least moderate. Proof for this is the convergence of the results with long bodies in comparison to the 2D-results of other authors, Vugts (1968) and Mei (1976). Although this thesis did not study forces in the intermediate depth water, the use of Garrison's program revealed that the results for these depths are not valid and there is some problem in the used version of the program.

Bibliography

- Volker Bertram. *Practical Ship Hydrodynamics*. Butterworth-Heinemann, 2 edition, 2012.
- A. H.-D. Cheng and D.T. Cheng. Heritage and early history of the boundary element method. *Engineering Analysis with Boundary Elements*, 2005.
- O.M. Faltinsen. *Sea Loads on Ships and Offshore Structures*. Cambridge University Press, 1990.
- C.J Garrison. Hydrodynamics of large objects in the sea part i - hydrodynamic analysis. *J. Hydronautics*, 8, 1974.
- C.J Garrison. Hydrodynamics of large objects in the sea part ii - motion of free-floating bodies. *J. Hydronautics*, 9, 1975.
- C.J Garrison. *Numerical Methods in Offshore Engineering*, chapter Hydrodynamic Loading of Large Offshore Structures. John Wiley Sons, 1978.
- C.J. Garrison. *Hydrodynamics of Large Displacement Fixed and Floating Structures in Waves*, 1980.
- Daniel Inman. *Engineering Vibration*. Prentice Hall, 2000.
- Joseph Katz and Allen Plotkin. *Low-Speed Aerodynamics*. Cambridge University Press, 2001.
- Jerzy Matusiak. *Dynamics of a Rigid Ship*. Aalto University, 2013.
- Chiang C. Mei. Power extraction from water waves. *Journal of Ship research*, 1976.
- J.N. Newman. *Marine Hydrodynamics*. The MIT press Cambridge, Massachusetts, and London, England, 1977.
- Ilkka Saisto. Vapaan nestepinnan ongelman ratkaisu reunaelementtimenetelmällä. Technical report, Helsinki University of Technology, Ship Hydrodynamics Laboratory, 1991.

- C. Truesdell. Notes on the history of the general equations of hydrodynamics. *The American Mathematical Monthly*, 60(7), 1953.
- Ir. J. H Vugts. The hydrodynamic coefficients for swaying, heaving and rolling cylinders in a free surface. *International Shipbuilding Progress*, 1968.
- D.F. Young, B.R. Munson, T.H. Okiishi, and W.W. Huebsch. *A Brief Introduction to Fluid Mechanics*. John Wiley sons, Inc., 2007.

Appendix A

Flap radiation pressures

The radiation pressures presented here are for the flap. Sway is the motion perpendicular to the length and in our coordinate-system along the x-axis. The results are presented for each length and for three chosen frequencies (already present before). For one frequency, the added mass and damping have a fixed scale, which has been chosen to match the maximum value of those two quantities. The presented pressures are made dimensionless and can be understood as a height ratio between the height of a water column (corresponding to the actual pressure) and the amplitude of the body motion.

FLAP, $\frac{p_{N11}}{\rho g x_1^0}$ at $\lambda = 15.7T$

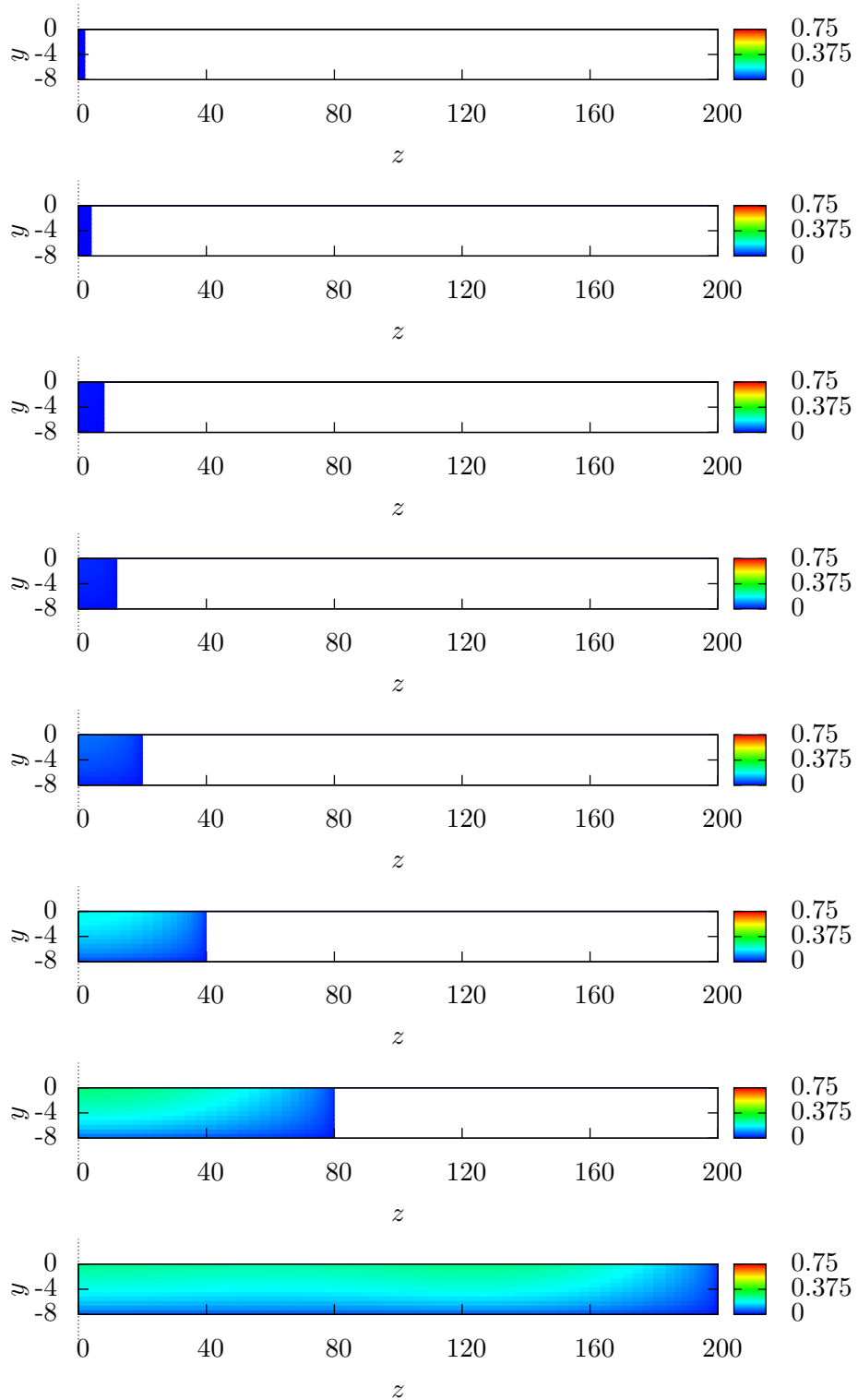


Figure A.1: Dimensionless sway damping distribution for flap when $\lambda = 15.7T$

FLAP, $\frac{p_{M11}}{\rho g x_1}$ at $\lambda = 15.7T$

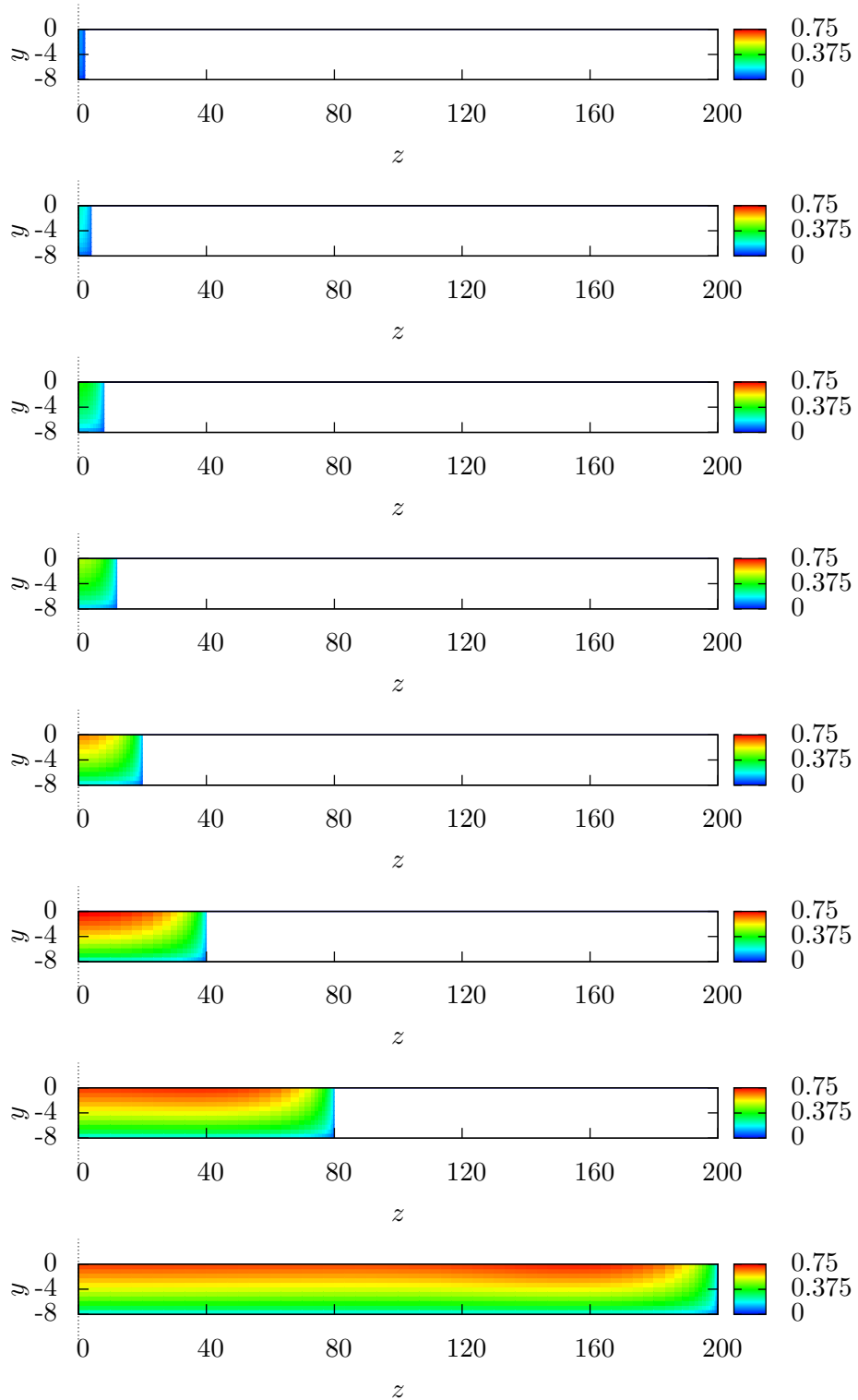


Figure A.2: Dimensionless sway added mass distribution for flap when $\lambda = 15.7T$

FLAP, $\frac{p_{N11}}{\rho g x_1^0}$ at $\lambda = 7.9T$

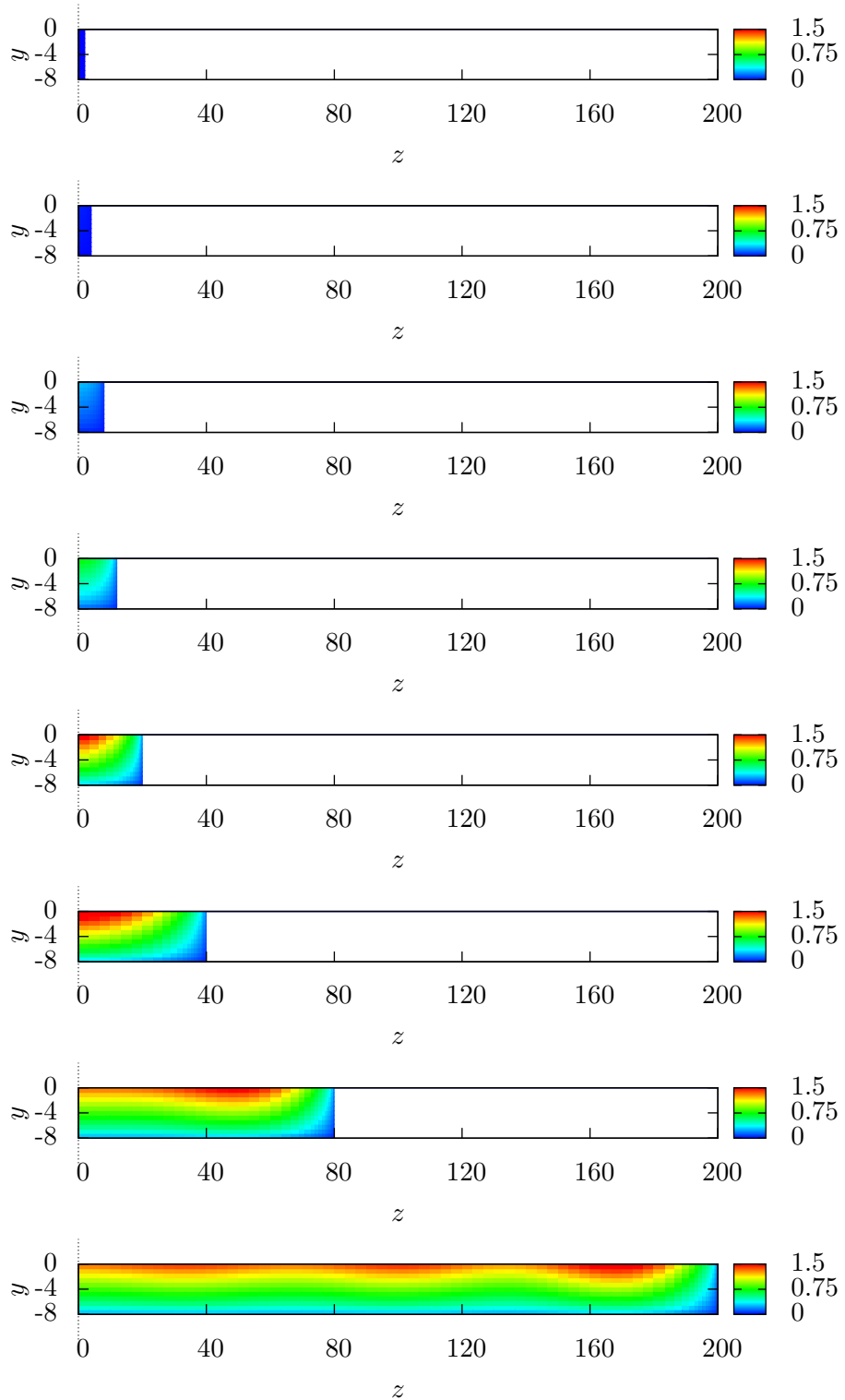


Figure A.3: Dimensionless sway damping distribution for flap when $\lambda = 7.9T$

FLAP, $\frac{p_{M_{11}}}{\rho g x_1^0}$ at $\lambda = 7.9T$

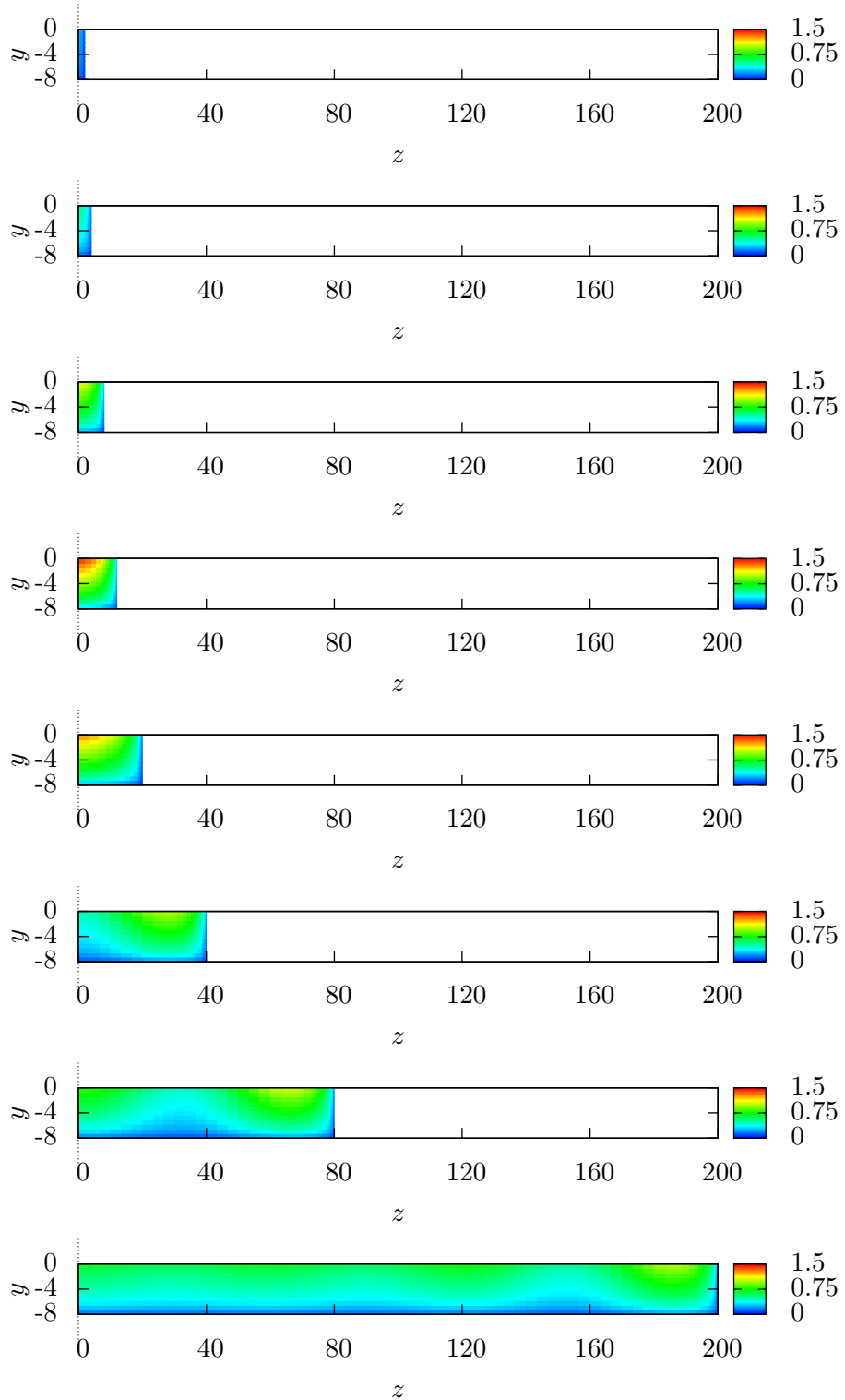


Figure A.4: Dimensionless sway added mass distribution for flap when $\lambda = 7.9T$

FLAP, $\frac{p_{N11}}{\rho g x_1^0}$ at $\lambda = 5.2T$

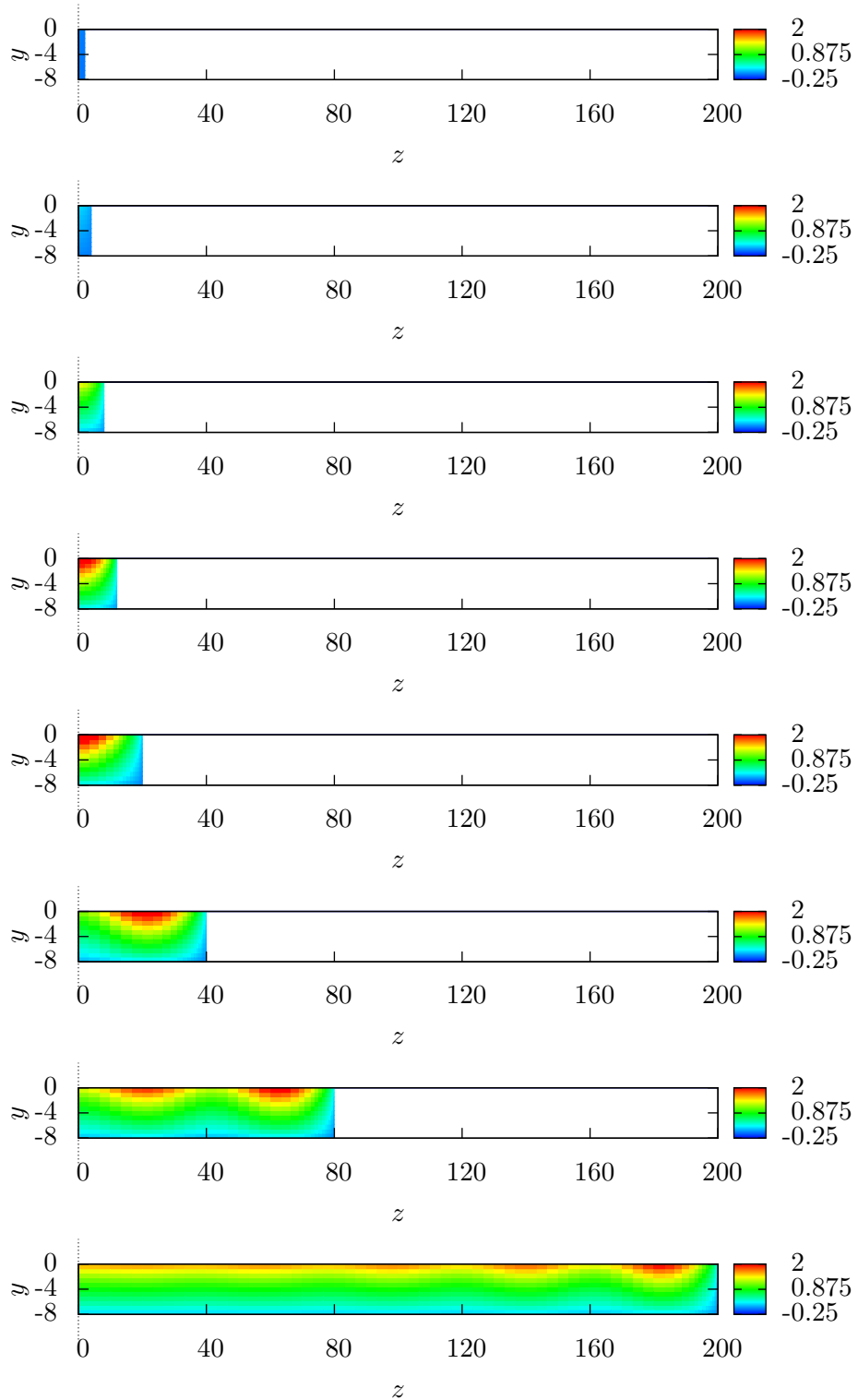


Figure A.5: Dimensionless sway damping distribution for flap when $\lambda = 5.2T$

FLAP, $\frac{p_{M11}}{\rho g x_1^0}$ at $\lambda = 5.2T$

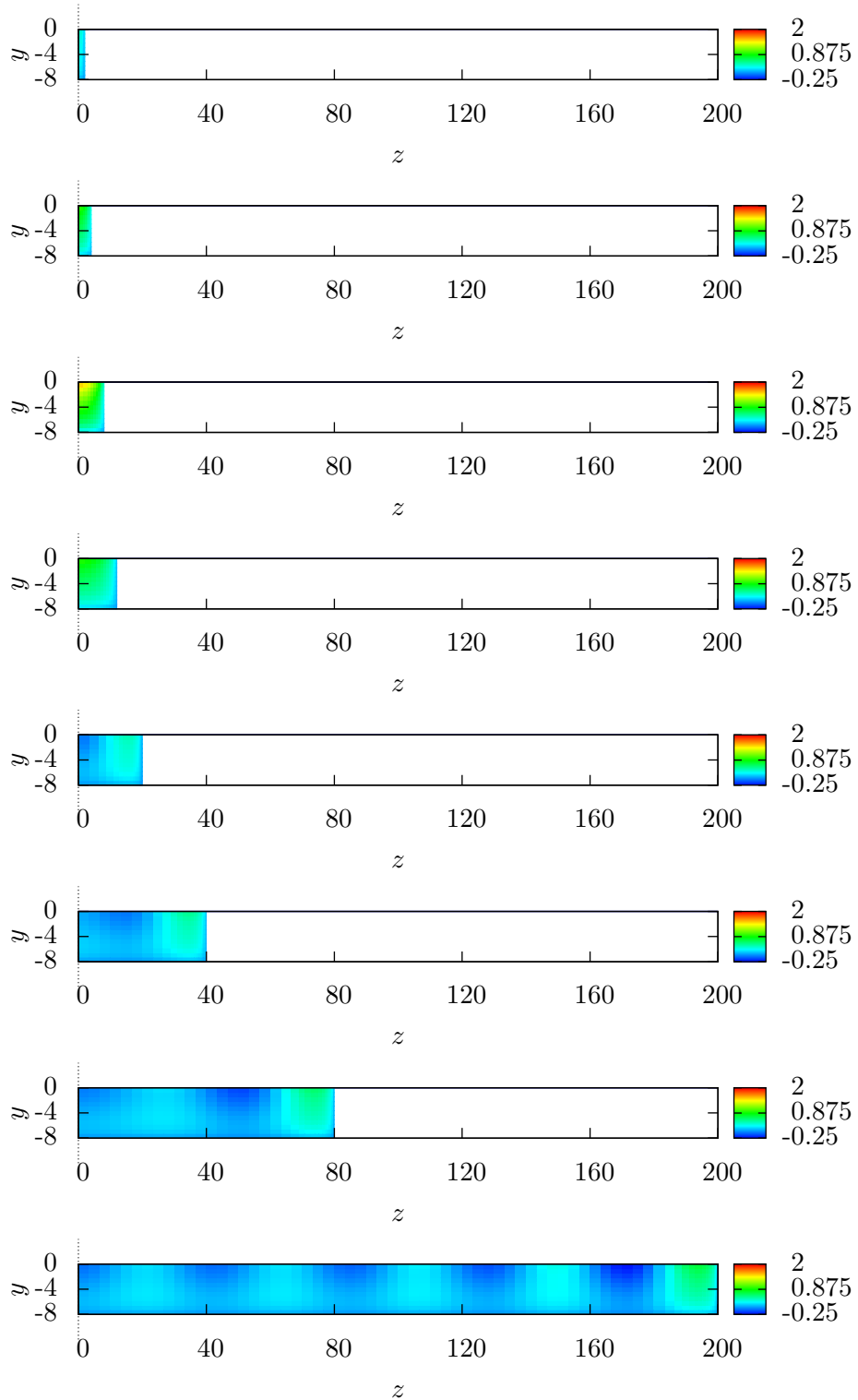


Figure A.6: Dimensionless sway added mass distribution for flap when $\lambda = 5.2T$